

We thank the editor and two anonymous referees for the comments and for giving us the chance to improve the manuscript. Below are our point-by-point responses to the referees' comments, followed by a revised manuscript showing all track changes made through the major revision.

Response to comments by anonymous referee #1:

Specific Comments:

Q1: L66-67: Reading back through the manuscript, this seems at odds with the practice of using single flux towers to represent the larger ecoregion (section 4.2). I don't actually have a problem with that research design, but this heterogeneity discussion may not be the best way to set things up.

Response: We have improved the discussion on using flux towers while trying to evaluate the effect of heterogeneity in the revised manuscript (L67-L73). We agree that flux towers are mainly installed and maintained at relatively flat areas and thus provide fluxes and meteorological conditions that are not indicative of the heterogeneity in each ecoregion. Still, we believe that HPM models trained at these sites can capture the interactions among ET, R_{ECO} and meteorological forcing and vegetation data and then reproduce at some extent the heterogeneity in ET and R_{ECO} within the ecoregion based on the variability in meteorological forcing and vegetation data. We validated this approach in the Use Case 2. While the results obtained in the various Uses cases show that the developed approach performed well, they also indicate the current limitations of this approach. The main limitation is due to insufficient resolution of meteorological reanalysis product, which did not reflect the corresponding heterogeneity. In addition, snow and soil moisture data could presumably improve HPM estimation especially during seasonally dry periods, however these datasets are difficult to be obtained over space and time. In the discussion section of the revised manuscript, we have also acknowledged ongoing research that focus on resolving data limitation issues caused by complex terrain, such as NASA's Asteroid Redirect Mission and Surface Atmosphere Integrated Field Laboratory Data.

Q2: L 73-75: Also uneven hydrologic distribution due to lateral flow in complex terrain (e.g., Chang et al. 2018) that results in heterogeneous fluxes.

Response: We have acknowledged this perspective (L83-L86).

Q3: L109: Has NDVI been defined?

Response: We have added the definition (L116).

Q4: L142-144; L365-367: After reading through the manuscript once, I'm not convinced this objective was met or even really addressed, which was confusing because I kept expecting to come across these results. The small-scale heterogeneity results must be expanded or else it may not be a fatal flaw to just remove this language/objective if the analysis didn't work out (as you intimate on L574-577). In any case, the current manuscript introduction/objectives/results are inconsistent with respect to the degree of focus on this topic.

Response: We agreed that the particular objective of reconstructing small-scale heterogeneity was not entirely met. While the method has shown promising results for predicting ET at other locations in similar topographic position (i.e., flat area), we intended to investigate how meteorological forcing and vegetation heterogeneity influence ET and R_{ECO} at the East River Watershed and the nearby SNOTEL stations. With comparison of meteorological forcing data between weather station and DAYMET data (Figure S3 and S4), we concluded that the insufficient resolution in meteorological reanalysis products limited the ability to estimate the spatiotemporal variability of ET and R_{ECO} in mountainous watersheds where slope aspect

influence the energy balance. This confirms the importance of improving meteorological reanalysis products. While we recognize the above limitation, the impact of vegetation on the ET and R_{ECO} dynamics can be assessed as NDVI data are obtained at much higher resolution. This is what we focused on in section 4.4. The objective and related discussions have been modified and clarified (L147-L152, L365-L374).

Q5: L143: Replace “CO” with “Colorado, USA” for the global audience.

Response: We have made this change (L151).

Q6: L150: I’m curious how you defined “mountainous watersheds” for this study. I’ve been to the Walnut Gulch sites and they didn’t strike me as the least bit mountainous. Also, with respect to my comment on L142-144, how important is the “mountainous” aspect anyway? I understand the broader impacts for water resources, but you’d reach a wider audience if the results were presented in a more general way. I see advantages and disadvantages to both mountain-specific and general analyses, but details/justification (mountain) or else re-framing (general) is needed in either case.

Response: We define mountainous watersheds as watersheds where different microclimate are present for different elevations (e.g., montane, subalpine and alpine areas). In this study, we mainly refer to the East River Watershed in Colorado, USA as the representative site for mountainous watersheds (Use Case 4).

The FLUXNET sites were selected to test HPM’s capability and limitations under different climate conditions, which may not necessarily locate in mountain regions. For example, US-Ton and the Walnut Gulch site should not be treated as mountainous watershed sites. We have justified these differences in revised manuscript (L158-L160, L162-L174).

Q7: L162: How were the eight FLUXNET stations selected? Some justification needed here. Was it to facilitate the paired approach in section 4.2?

Response: The Fluxnet sites were selected to sample different climate type, cover a wide range of meteorological and vegetation conditions, and provide continuous >5 years’ time series data. These sites represent different ecoregions from Californian Mediterranean, Sierra Madre Piedmont to Western Cordillera and Boreal Plain. Using sites in various ecosystems enabled us to evaluate the performance of HPM across different sites located in the same ecoregion and evaluate differences in processes driving the ET and R_{ECO} response in various ecoregions. For example at ecoregions limited by energy conditions (e.g., CA-Oas), current HPM estimations are good, whereas at ecoregions with seasonally dry periods, additional variables (e.g., soil moisture data) might be needed to improve HPM accuracy. The choices of these sites not only facilitated the paired approach in Use Case 2 and 4, but also enabled us to assess HPM limitations at different ecoregions. In the recent revision of the manuscript, additional sets were considered, including US-Me2 (Q21).

Q8: L164: Table 1 indicates that the Saskatchewan sites are colder than US-NR1.

Response: We have corrected this mismatch (L164).

Q9: Table 1: I assume the periods of records are truncated at 2015 because you used the FLUXNET2015 product? This should be specified. Watch significant figures through-out this table.

Response: Yes. We have clarified this point in the revised manuscript (L187).

Q10: L227: Why was it necessary to treat this site different than the others? Please provide details about this “cleaning” procedure and why it was needed.

Response: We have identified some data gaps and erroneous data for the ET data at US-NR1 from the FLUXNET2015 database. The data cleaning framework provided in Rungee et al., 2019 is well documented. We made this decision after visualizing the raw data at US-NR1, where measurements during winter periods are likely uncertain. (L229-L230)

Q11: L367: The previous text makes it sounds like three (nor four) cases – confusion.

Response: Thank you for your comment. We have clarified the paragraph (L365-L371).

Q12: Table 3: You probably don't need a table just to say that "sn" was included at three of the eight sites. Especially because you already have so many display items.

Response: Thank you for your comments. We have made the recommended change.

Q13: L378-380: I'm very curious as to whether this was also the case at the seasonally dry Walnut Gulch sites? If so, it speaks to systematic bias where the model captures ET dynamics during energy-limited but not water-limited periods. This strikes me as a major result (see general comments) and could be leveraged to make recommendations about the input variables that are necessary for various systems.

Response: Thank you for your comments. We agree that the current HPM models with only meteorological attributes and NDVI as features generally captures ET dynamics during energy-limited but not water-limited periods. Variables (i.e., precipitation and constructed index, *sn*) provide indirect information regarding water stress, and we have observed high prediction accuracy during winter time and early growing season. However prediction accuracy usually decreases during peak growing season (summer time), especially at ecoregions that experience dry periods (e.g., occurrence of drought (Sloat et al., 2015; Wainwright et al., 2020). Based on these observations, HPM performs better during energy-limited periods than water-limited periods. As soil moisture is the variable that directly quantifies subsurface moisture stress, including soil moisture as a key variable at HPM can be effective in improving HPM performance. However, soil moisture data highly depends on depth and other subsurface properties (more details provided in Q19). Due to these reasons, we decided not to include soil moisture at the current stage for HPM development (L333-L338) and emphasized the importance of including necessary variables when data becomes available for various systems (L616-L627).

Q14: L383-395: Wouldn't the model overestimate (not underestimate) Reco if it can't account for soil moisture limitation during this time? Please clarify

Response: LSTM captures the long-term temporal fluctuations over time really well. But less frequent signals from peak growing season can be neglected due to the decreasing statistical significance. The underestimation of R_{ECO} during peak growing season is resulted from LSTM emphasizing on capturing long term dynamics and smoothing the larger values that occur less frequently.

Q15: L408-411: Seemingly contradicts L66-67

Response: We have further clarified this bullet point in the revised manuscript (L65-L73). Also see response for Q1 response.

Q16: L493: Units mismatch

Response: We have made the necessary correction (L519-L520).

Q17: L495-505: Discussion

Response: We have made the necessary changes.

Q18: L516-518: In my mind, this is a missed opportunity to gain processed-based (and thus transferrable) insight. What about these sites could factor into ET differences that are so much greater than the Reco differences? See general comments.

Response: Thank you for your comment. Through further investigating data inputs and model performance, we believe the ET and R_{ECO} estimation at the East River Watershed are limited by the insufficient resolution of input data. There are two major factors that lead to the differences of ET and R_{ECO} among these sites. The first perspective is that HPM ET model is more sensitive to temperature and radiation inputs compared to NDVI whereas NDVI, temperature and radiation are all influential for R_{ECO} estimations. The second perspective is about data resolution and uncertainty. Data provided by SNOTEL weather stations are more accurate than DAYMET reanalysis data. We observed a greater differences in temperature and radiation at the SNOTEL sites whereas there's very small differences at the East River sites (Figure S3). Summer temperature differences among SNOTEL sites can be over 3°C but there's a barely 0.2°C differences in DAYMET data used for the East River sites. From Landsat data, we could distinguish the differences in NDVI at the East River sites (Figure 10) and these differences are well captured by HPM R_{ECO} model. Considering both the model and data perspectives, it explained why we observed these differences in ET and R_{ECO} at these sites. With the high prediction accuracy for Use Case I scenarios, we believe HPM is capable to capture the interactions among ET, R_{ECO} and input variables. If high resolution meteorological data becomes available at the East River Watershed such as the Surface Atmosphere Integrated Field Laboratory (SAIL), we believe HPM can better distinguish how meteorological forcing heterogeneity controls ET and R_{ECO} and more process-based interpretation can be learned from HPM estimations. These discussions have been implemented in the revised manuscript (e.g., L535-L551; L597-L604; L628-L637).

Q19: L544-546: How hard would it be to add moisture into the model? Why wasn't it added in the first place? I'm not suggesting that you re-do the analysis, but the readers will be very interested in this information.

Response: For Use Case 1 situations, it is applicable and relatively easy to add soil moisture into the model. However for the other Use Cases where the model will be transferred over space, it is difficult to directly use soil moisture as an input variable given soil moisture measurements is often made at various depths, and other aquifer characteristics that won't necessarily be the same at different sites. This dependence on depth and other soil characteristics limits the model transferability at inadequately monitored watersheds (L333-L338). Thus we have decided not to include soil moisture as an input variable. In L616-L627 of the revised manuscript, we have recommended to include soil moisture and other important variables if data becomes available and researchers have more information regarding the site of focus. For example, at ecoregions that experience seasonally dry periods, it is useful to add soil moisture in HPM.

Q20: L563-568: It's not clear to me what model results "present similar dynamic trends" to the moisture limitation invoked by Hu et al. 2010 (and a host of larger scale, more recent work). My current understanding is that the model breaks down somewhat in the presence of moisture limitation, which I consider an interesting and valid result/contribution, but you can't have it both ways i.e., the model either does or does not capture fluxes during periods of relative moisture limitation. Perhaps I'm missing something.

Response: Thank you for your comment. We meant to say ET and R_{ECO} estimation from HPM at the East River Watershed are comparable to the other studies. Specifically in Hu et al. (2010) at US-NR1, they were able to use snow, branch and soil sample data to conclude longer growing season lead to less carbon sequestration. At the East River Watershed, HPM estimated smaller R_{ECO} for evergreen forest (592 to 639 gCm^{-2}) that have longer growing season, compared to deciduous forest (642 to 698 gCm^{-2}). In the

revised manuscript, we also compared 2012 (earlier snowmelt and longer growing season length) to other years and discussed how these dynamics influence seasonal and annual ET and R_{ECO} (L521-529).

The current HPM model does not include soil moisture due to reasons in Q19, however other attributes, such as precipitation and sn, provide indirect information regarding the moisture inputs. Thus fluxes estimated from HPM during moisture limiting periods are still reasonable. In the revised manuscript, we have demonstrated this limitation of HPM and suggested to incorporate soil moisture data in addition to precipitation and sn when they become available.

Q21: L609: Still need more convincing about how “mountainous” was defined and why these sites were chosen, in particular with respect to other “mountainous” sites in the FLUXNET2015 database. I’m thinking of sites in New Mexico and possibly Oregon off the top of my head.

Response: Thank you for your comment. In our study, the representative site of mountainous watersheds is the East River Watershed, and the surrounding US-NR1 and SNOTEL sites. Other Fluxnet sites were selected to test the capability and limitations of HPM under other climate conditions (e.g., US-Ton, US-Wkg) and are not considered as mountainous sites. We have also included US-Me2 (Oregon) in our study. We did not include US-VCM (New Mexico site) after recognizing the occurrence of fire in 2013. These changes have been clarified in the revised manuscript. We have also added the estimation of ET and R_{ECO} at US-Me2. Results of US-Me2 is attached here and also included as Figure A5 in the revised manuscript.

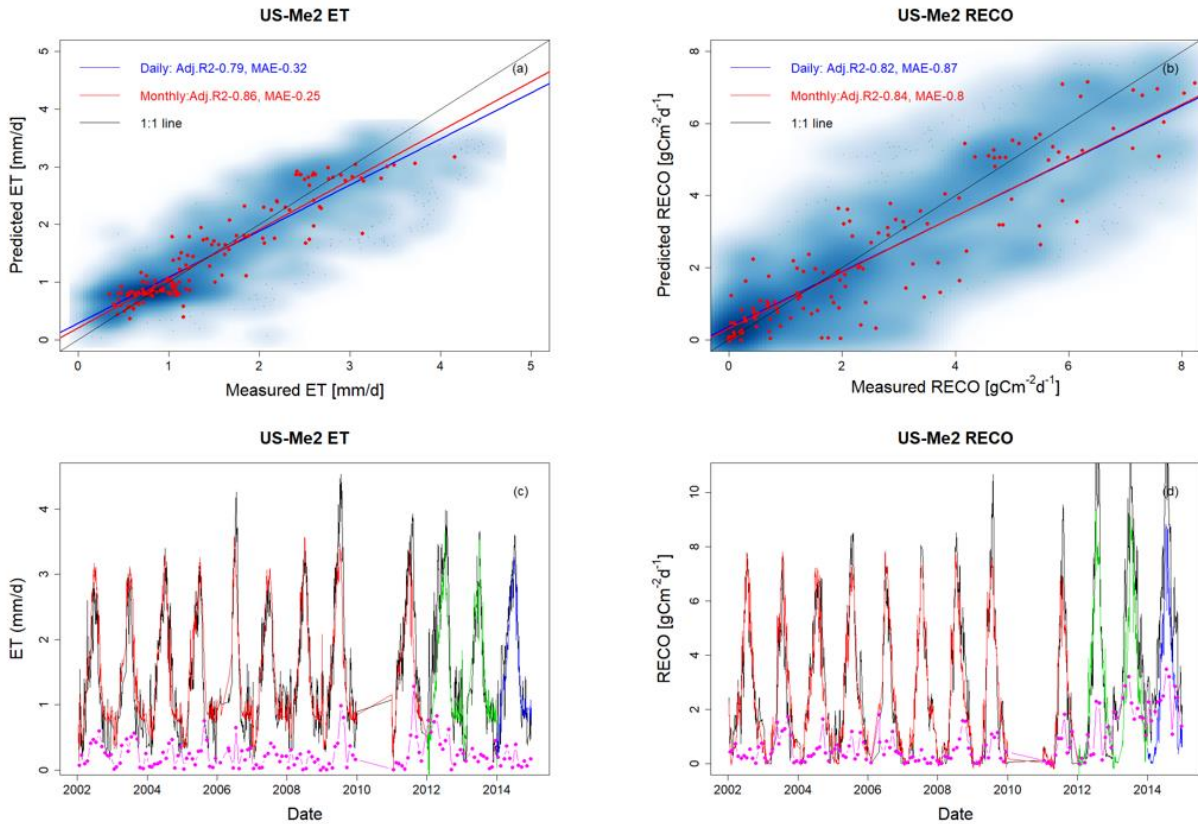


Figure 1. Added HPM estimation of ET and R_{ECO} at US-Me2. Data from 2011 are partially missing, which may decrease LSTM performance at US-Me2.

Response to comments by anonymous referee #2:

Q1: Row 34: why Reco? I can't understand why the second variable considered in the study was the ecosystem respiration. It is not observed directly by FLUXNET network, but can be estimated indirectly from net ecosystem exchange (NEE) measurements made by eddy covariance towers during the night. The main term is NEE, why are you not considering it directly? NEE is the key variable considered world wide. Please, include NEE.

Response: We agree that NEE is one of the key variables considered worldwide, and is directly measured by eddy covariance flux towers. However, R_{ECO} is also very important as it represents the total ecosystem carbon emissions from land to the atmosphere, and is very sensitive to climate change (Le Quéré et al., 2009), and thus quantifying and estimating R_{ECO} is needed. This study is not the only one that concentrates on R_{ECO} . For example, Ai et al. (2018) developed a semi-empirical, physiologically based, remote sensing model to estimate R_{ECO} using MODIS data; Solomon et al. (2013) estimated daily respiration rates using maximum likelihood fits of a free-water metabolism to quantify respiration dynamics in six lakes.

An additional reason to consider R_{ECO} and not NEE in this study is that one of the major objectives of this study is to provide an estimate of ET and R_{ECO} at watersheds where flux towers are not available. The daytime and nighttime partitioning methods (van Gorsel et al., 2009; Reichstein et al., 2005) requires sub-daily scale NEE data to compute daily scale R_{ECO} . However at these sparsely monitored watersheds, sub-daily scale NEE data is not available and could not be predicted with weather reanalysis and remote sensing data that are at coarser temporal scales. Thus developing methods that estimate daily scale R_{ECO} is still needed and will help advance our understanding of ecosystem dynamics and carbon cycling at the inadequately monitored watersheds.

While we decided to not include NEE in our manuscript, we have tested the HPM approach to estimate NEE at CA-OAS. We observed a R^2 larger than 0.8 between the measurements and predictions (Figure 2). With this result, we believe HPM can be an appropriate approach for estimating daily NEE with right choices of variables. However, we believe replacing R_{ECO} with NEE will change the scope of this study, and thus we do not plan to include NEE at the current stage.

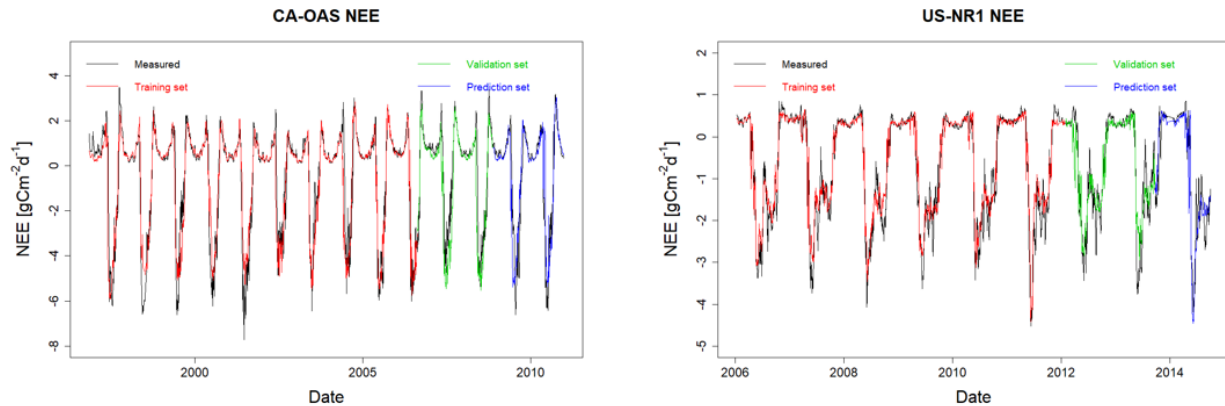


Figure 2. HPM estimate of NEE at CA-OAS and US-NR1. R^2 between estimation and measurements are 0.87, 0.83 and 0.81 at CA-OAS; 0.94, 0.88 and 0.90 at US-NR1 for the training set, validation set and prediction set, respectively. Model inputs include air temperature, soil temperature, sn, precipitation and radiation.

Q2: Rows 101-105: please, include also SENTINEL 2, the new satellite for NDVI observations with better time and spatial resolutions, available from 2015.

Response: We considered using SENTINEL 2 data but our evaluation has shown that LANDSAT was more adapted for the period of time we are concentrating on in this study. From our knowledge, the Sentinel 2 surface reflectance data has a 10m resolution for the red and near infrared band with an averaged revisit time of 5 days since March 2017 (Main-Knorn et al., 2017). In Use Case I, II and III scenarios, our HPM estimates covered the period up to 2016 as we were using FLUXNET2015 datasets. For Use Case IV, we have checked the data availability of Sentinel 2 surface reflectance data over the East River Watershed. A total of 106 Sentinel 2 dataset is available till 2018, however only 13 of them have a cloud cover less than 10% during the sampling period. We tested with the additional Sentinel-2 NDVI data, but we did not observe notable changes in ET and R_{ECO} estimations compared to previous ones with only Landsat data. Meanwhile, we also checked out other satellite products, including the Planet-Lab (McCabe et al., 2017); the harmonized Landsat-Sentinel product (Claverie et al., 2018) as well as other satellite data fusion products (Shao et al., 2019). However, they still do not increase the temporal resolution prior to 2017. Based on the above assessment we decided to use Landsat data only. We agree that future work could expand HPM based ET and R_{ECO} estimations using various combination of satellite products.

Q3: Rows 162-165: mean annual precipitation of the watershed is 1200 mm/y. Hence, how can be representative these stations?

Response: We agree the manuscript did not clearly describe the reason of using FLUXNET site with very different meteorological forcing from the East River watershed. We have improved the manuscript to make it clearer. The FLUXNET sites considered in this study is mainly used in Use Case I and Use Case II. We wanted to explore the capability of HPM under different climate conditions. For example, we selected US-Ton to test whether HPM is able to provide reasonable estimate of ET and R_{ECO} under Mediterrean climate (Csa) whereas at US-NR1 for subarctic environment (Dfc). We did not intend to use HPM developed at US-Ton and other FLUXNET sites to be representative stations for the East River Watershed. We have further clarified the major objective of and the various Use Cases in the revised manuscript (L166-L174, L365-L374).

Q4: Rows 194-196: basin areas? slope?

Response: We were describing the general characteristic of the East River Watershed, which include both basin areas and montane areas.

Q5: Rows 207: why 16 locations? And not 10 or 20? Please, any sensitivity analysis? Any uncertainty estimate?

Response: We focused on four main vegetation types within the East River Watershed, including deciduous forests, evergreen forests, riparian shrublands and meadow grasslands. We defined 16 locations to have some replicates to evaluate the spatial variability. Given the 30-m spatial resolution of Landsat, we tried to select locations at the center of vegetation patched and covered or at least strongly dominated by one vegetation type. We evaluated it manually and decided that 16 locations (4 for each vegetation type) was a pragmatic choice.

Equation (1): this equation is the NDVI definition, you don't need to include in the text, it is well known.

Response: We have made the necessary change in the revised manuscript.

Q6: Row 264: please, include the time resolution of the model, its space resolution, and the size of the domain.

Response: The time resolution of HPM is daily. The spatial resolution depends on different Use Cases and spatial resolution of data inputs. We have made these changes in the revised manuscript, and also further clarified in each of the Use Cases in section 4 (L371-L374).

Q7: Row 291: how is estimated g ?

Response: g is the hyperbolic tangent activation function. It is used to determine candidate cell states and update the hidden states (Hochreiter and Schmidhuber, 1997; Kratzert et al., 2019). g is not estimated.

Q8: Row 300: how are estimated W_f , U_f , and b_f ?

Response: We clarified this. W_f , U_f and b_f are representing learnable parameters for the forget gates. There are other W , U and b for the internal states and hidden states. We used the Adam algorithm (Kingma and Ba, 2014) with a mean absolute error loss function built in Keras (Chollet, 2015).

Q9: Row 318: how many parameters in total?

Response: We thank the reviewer's comment. There are 11600 and 7600 parameters for the first and second LSTM layers; 208 and 9 for the first and second dense layers and no parameters for the dropout layers. These information is available in Table 1 in the supplementary material.

Q10: Equations (10) and (11): you don't need to include these equations. These are statistical index very well known.

Response: We have made the necessary change in the revised manuscript.

Q11: Row 362-363: I looked at section 4.1 and it doesn't estimate any temporal dependency. It just tested the model at a not very clear time scale.

Response: We used the word "long term temporal dependency" in a deep learning (or statistical) context where there are significant temporal correlation and long time lags in time series. LSTM and recurrent neural networks are one of the very efficient and effective deep learning models that are capable to capture such long term dependencies. In the revised manuscript, we have been more careful in terms of the wording that overlap among different fields.

Q12: Row 374: again, what is the time scale?

Response: We thank the reviewer's comment. Our ET and R_{ECO} estimations are at daily scale. We have better clarified the time scale in the manuscript.

Q13: Row 390: Is it always at monthly time scale? please, again, define the time scale.

Response: We thank the reviewer's comment. Our estimate is at daily scale, which are used to calculate monthly means. In figure 5 and following figures, we presented the results of both daily and monthly mean between HPM and measurements in order to check model performance. We also aggregated our daily estimates to 8-day mean at the East River sites, which enabled us to compare our results to Mu et al. (2013) as shown in Figure S1

Q14: Row 396-307, "...which also indicates that soil moisture data is necessary to increase Reco prediction accuracy in this ecoregion...". how can you support this statement?

Response: We thank the reviewer's comment. The decreasing prediction accuracy occurred at sites limited by water and moisture conditions (e.g., US-Ton and US-Var) where other studies investigated how ecosystem respond to subsurface water availability (Von Buttlar et al., 2018; Song et al., 2014). At sites with seasonally dry periods (e.g., US-NR1), other studies have also identified the occurrences of fore-summer drought and water limiting condition (Sloat et al., 2015; Wainwright et al., 2020). Due to practical reasons, current HPM models did not include soil moisture as an input to capture these seasonally dry periods. Thus we believe modified HPM models with soil moisture as inputs can increase prediction accuracy in these ecoregions when soil moisture data becomes more available in space and time.

Q15: Row 415: Are the model parameters changing for each site? What are the parameter values?

Response: We thank the reviewer's comment. Deep learning parameters for US-Ton, CA-Oas and US-Wkg are different as they are three different developed HPM models used to represent different ecoregions. As mentioned in the response to Q9, there are many deep learning parameters and it is not feasible to directly present the values of these learnable parameters here. But all of these parameter values are available in the data package we submitted to ESS-DIVE and can be downloaded at <https://data.ess-dive.lbl.gov/view/doi:10.15485/1633810> named 'LSTM_model.zip'.

Q16: Row 419-420: I don't agree, Reco predictions are not good in US Whs and US Var

Response: We thank the reviewer's comment. HPM achieved a daily scale adjusted R^2 of 0.70 and 0.78 and MAE at 0.67 and 0.22 at US-Whs and US-Var respectively, in Use Case II scenario. We agree that the statistical measure is not as satisfactory as R^2 over 0.9. In the revised manuscript, we have made the necessary changes correspondingly (L430-L433).

Q17: Row 518-519, "This result indicates small-scale meteorological forcing and vegetation heterogeneity are the major controls of differences in ET and Reco at the East River Watershed": please, highlight and clarify what is the new finding. We know already that meteorological forcing (which is the model input), and vegetation heterogeneity (model parameter) are the controlling factors of the model.

Response: We thank the reviewer for the comment. We have expanded our discussion on how ET and R_{ECO} dynamics vary at different years (e.g., years with earlier snowmelt versus later snowmelt). We have emphasized how vegetation types contribute to ET and R_{ECO} spatiotemporal heterogeneities. We also discussed the limitations and practical perspectives of current HPM models in feature selection and how to improve estimation accuracy at seasonally dry periods. In addition, we clarified the role of meteorological forcing attributes and vegetation types in ET and R_{ECO} dynamics at the East River Watershed and tested how these input variables contribute to ET and R_{ECO} differences at different years among different sites. These findings have been revised in the result and discussion sections.

Q18: Row 673: please add the journal name of this reference, I can't find it.

Response: We thank the reviewer's comment. The journal name of this reference is 'Journal of Geophysical Research: Biogeosciences' (L727-L730). We have double checked and made sure the bibliography is correctly and clearly presented.

A Deep-Learning Hybrid-Predictive-Modeling Approach for Estimating Evapotranspiration and Ecosystem Respiration

Jiancong Chen¹, Baptiste Dafflon², Anh Phuong Tran^{2, 3}, Nicola Falco², and Susan S. Hubbard²

¹Department of Civil and Environmental Engineering, University of California, Berkeley, CA, USA, ²Earth and Environmental Sciences Area, Lawrence Berkeley National Laboratory, Berkeley, CA, USA, ³Department of Water Resources Engineering and Technology, Water Resources Institute, 8, Phao Dai Lang, Dong Da, Hanoi, Vietnam

Abstract: Gradual changes in meteorological forcings (such as temperature and precipitation) are reshaping vulnerable ecosystems, leading to uncertain effects on ecosystem dynamics, including water and carbon fluxes. Estimating evapotranspiration (ET) and ecosystem respiration (R_{ECO}) is essential for analyzing the effect of climate change on ecosystem behavior. To obtain a better understanding of these processes, we need to improve our estimation of water and carbon fluxes over space and time, which is difficult within ecosystems ~~where we that often~~ have only sparse data. In this study, we developed a hybrid predictive modeling approach (HPM) that integrates eddy covariance measurements, physically-based model simulation results, meteorological forcings, and remote sensing datasets to estimate evapotranspiration (ET) and ecosystem respiration (R_{ECO}) in high space-time resolution. HPM relies on a deep learning algorithm-long short term memory (LSTM)-as well as direct measurements or outputs from physically-based models. We tested and validated HPM estimation results at sites within various sites. We particularly focus on testing HPM in mountainous regions, given their importance for water resources, their vulnerability to climate change, and the recognized difficulties in estimating ET and R_{ECO} in ~~mountainous~~such regions. We benchmarked daily scale estimates of ET and R_{ECO} obtained from the HPM method against measurements made at FLUXNET stations and outputs from the Community Land Model (CLM) at Rocky Mountain SNOTEL stations. At the mountainous East River Watershed site in the Upper Colorado River Basin, we explored how ET and R_{ECO} dynamics estimated from the new HPM approach vary with different vegetation and meteorological forcings. The results of this study indicate that HPM is capable of identifying complicated interactions among meteorological forcings, ET, and R_{ECO} variables, as well as providing reliable estimation of ET and R_{ECO} across relevant spatiotemporal scales~~-, even in challenging mountainous systems.~~ With HPM estimation of ET and R_{ECO} at the East River Watershed, we ~~found~~identified that ~~abiotic factors of HPM ET models are sensitive to~~ temperature and radiation ~~predominantly explained ET spatial variability; inputs~~ whereas NDVI, temperature and radiation all have crucial influences over R_{ECO} ~~variability was largely controlled by biotic factors, such as vegetation type dynamics.~~ In general, our study demonstrated that the HPM approach can circumvent the typical lack of spatiotemporally dense data needed to estimate ET and R_{ECO} over space and time, as well as the parametric and structural uncertainty inherent in mechanistic models. While the current limitations of the HPM approach are driven by the temporal and spatial resolution of available datasets (such as meteorological forcing and NDVI data), ongoing advances ~~in remote sensing~~ are expected to further improve accuracy and resolution of ET and R_{ECO} estimation using HPM.

1. Introduction:

Evapotranspiration (ET) and ecosystem respiration (R_{ECO}) are key components of ecosystem water and carbon cycles. ET is an important link between the water and energy cycles: dynamic changes in ET can affect

precipitation, soil moisture, and surface temperature, leading to uncertain feedbacks in the environment (Jung et al., 2010; Seneviratne et al., 2006; Teuling et al., 2013). Thus, quantifying ET is particularly essential for improving our understanding of water and energy interactions and watershed response to abrupt and gradual changes in climate, which is critical for water resources management, agriculture, and other societal benefits (Anderson et al., 2012; Jung et al., 2010; Rungee et al., 2019; Viviroli et al., 2007; Viviroli and Weingartner, 2008). R_{ECO} ~~describes, which represents~~ the sum of autotrophic respiration and respiration by heterotrophic microorganisms in a specific ecosystem ~~and,~~ plays a vital role in the response of terrestrial ecosystem to global change (Jung et al., 2017; Reichstein et al., 2005; Xu et al., 2004). As long term exchanges in R_{ECO} have pivotal influences over the climate system (Cox et al., 2000; Gao et al., 2017; IPCC, 2019; Suleau et al., 2011), approaches are needed to estimate and monitor R_{ECO} over relevant spatiotemporal scales. As described below, there are many different strategies for measuring and estimating ET and R_{ECO} , each of which has advantages and limitations. The motivation for this study is the recognition that current methods cannot provide ET and R_{ECO} at space and time scales (e.g., daily) needed to improve prediction of changing terrestrial system behavior, particularly in challenging mountainous watersheds.

Several ground-based approaches have been used to provide *in situ* estimates or measurements of ET and R_{ECO} . Ground based flux chambers capture and measure trace gases emitted from the land surface, which can be used to estimate ET and R_{ECO} (Livingston and Hutchinson, 1995; Pumpanen et al., 2004). However, the microclimate of the environment is affected by the chamber, and the laborious acquisition process and small chamber size typically lead to information with coarse spatiotemporal resolution (Baldocchi, 2014). The eddy covariance method uses a tower with installed instruments to autonomously measure fluxes of trace gases between ecosystem and atmosphere (Baldocchi, 2014; Wilson et al., 2001). The covariance between the vertical velocity and mixing ratios of the target scalar is computed to obtain the fluxes of carbon, water vapor, and other trace gases emitted from the land surface. ET is then calculated from the latent heat flux, and R_{ECO} is calculated from the net carbon fluxes using night-time or daytime partitioning approaches (van Gorsel et al., 2009; Lasslop et al., 2010; Reichstein et al., 2005). The spatial footprint of obtained fluxes is on the order of hundreds of meters, and the temporal resolution of the measurements range from hours to decades (Wilson et al., 2001). Such *in situ* measurements of fluxes have been integrated into the global ~~network of~~ AmeriFlux (<http://ameriflux.lbl.gov/>) and FLUXNET (<https://FLUXNET.fluxdata.org/>) ~~networks,~~ where such data have ~~strongly supported scientists in greatly benefited~~ process ~~understanding investigations~~ and model development. ~~Given undertaken by a wide scientific community. However, given~~ the cost, ~~effort~~ ~~effort~~, and power required to install and maintain a flux tower, eddy covariance towers are typically sparse relative to the scale of study sites used to address ecosystem questions. Additionally, the location of a flux tower within a watershed greatly influences measurement representativeness. For example, ~~for logistical reasons,~~ eddy covariance towers are usually installed at valley bottoms of mountainous watersheds (Strachan et al., 2016), ~~and estimates obtained there may not be representative of fluxes across a range of elevations or slope aspects within the watershed. The limited number of towers and their limited ability to sample different portions of a watershed thus limit the usefulness of flux towers for estimating ET and R_{ECO} in high resolution over space and time.~~ However, microclimate caused by complex mountainous terrains (e.g., slope, aspect and elevation) can have different radiation inputs and moisture dynamics compared to flat areas where flux towers are mostly installed. Flux measurements from eddy covariance towers

provide a representation of major driver and controls on ET and R_{ECO} in an ecoregion while meteorological forcing variability needs to be accounted to possibly represent various aspects introduced by complex terrain. Thus, though measurements from a single flux tower may not capture heterogeneity in ET and R_{ECO} due to complex terrain, they support the development of statistical or physical-based models integrated with other types of data to provide ET and R_{ECO} estimation in high resolution over space and time.

Physically-based models, which numerically represent land-surface energy and water balance, have also been used to estimate ET and R_{ECO} (Tran et al., 2019; Williams et al., 2009). These physically-based models solve physical equations to simulate the exchanges of energy, heat, water and carbon across atmosphere-canopy-soil compartments. Examples include the Community Land Model (CLM, Oleson et al., 2013). Performance of these models depend on the accuracy of inputs and parameters, such as soil type and leaf area index, which can be difficult to obtain at sufficiently high spatiotemporal resolution. The lack of measurements to infer parameters needed for models often leads to large discrepancies between model-based and flux-tower-based ET and R_{ECO} estimates. Conceptual model uncertainty inherent in mechanistic models can also lead to ET and R_{ECO} estimation uncertainty and errors. For example, Keenan et al. (2019) suggested that current terrestrial carbon cycle models neglect inhibition of leaf respiration that occurs during daytime, which can result in a bias of up to 25%. Chang et al. (2018) used virtual experiments with 3-D terrestrial integrated modeling system to investigate why a lower ratio of transpiration to ET is always produced by large scale land surface models. Their study suggested heterogeneous fluxes caused by uneven hydraulic distribution due to complex terrain are not always considered in process-based models. These conceptual uncertainties, in addition to data sparseness and data uncertainty, further limit the applicability of physically-based models to estimate ET and R_{ECO} at high spatiotemporal scales. Semi-analytical formulations based on combinations of meteorological and empirical parameters provide a reference condition for the water and energy balance. Examples used to estimate potential ET include the Budyko framework and its extensions (Budyko, 1961; Greve et al., 2015; Zhang et al., 2008); the Penman-Monteith's equation (Allen et al., 1998), and the Priestley-Taylor equation (Priestley and Taylor, 1972). Actual ET can then be approximated by multiplying a coefficient associated with water deficit (De Bruin, 1983; Williams & Albertson, 2004). However, even with these empirical formulations many attributes are still difficult to obtain globally at high temporal scales, such as water-vapor deficit, leaf area index, and aerodynamic conductance of different plants.

Remote sensing products, such as Landsat imagery (Irons et al., 2012), Sentinel-2 (Main-Knorn et al., 2017) and the moderate-resolution imaging spectroradiometer (MODIS, NASA, 2008), have also been integrated to estimate ET and R_{ECO} with empirical, statistical, or semi-physical relations (Abatzoglou et al., 2014; Daggers et al., 2018; Mohanty et al., 2017; Paca et al., 2019). Due to the high spatial coverage of remote sensing products, global-scale estimates of ET and R_{ECO} have become feasible. For example, Ryu et al. (2011) proposed the Breathing Earth System Simulator approach, which integrates mechanistic models and MODIS data to quantify ET and GPP with a spatial resolution of 1-5 km and a temporal resolution of 8 days. Ai et al. (2018) extracted enhanced vegetation index, fraction of absorbed photosynthetically active radiation, and leaf area index from the MODIS dataset—and used the rate-temperature curve and strong correlations between terrestrial carbon exchange and temperature to estimate R_{ECO} at 1

km spatial resolution and 8-day temporal resolution. Ma et al. (2018) developed a data fusion scheme that fused Landsat-like-scale datasets and MODIS data to estimate ET and irrigation water efficiency at a spatial scale of ~100 meters. However, even though remote sensing data cover large areas of the earth surface, they typically do not provide information over both high spatial and temporal resolution, and are also subject to cloudy conditions. For example, Landsat has average return periods of 16 days with a spatial resolution of 30 m (visible and near-infrared), whereas MODIS has 1-2 days temporal resolution with a 250 m or 1 km spatial resolution depending on the sensors. These resolutions are typically too coarse to enable exploration of how aspects such as plant phenology, snowmelt, and rainfall impact integrated ecosystem water and energy dynamics.

Combining machine-learning models with remote sensing products and meteorological inputs offers another option for large-scale estimation of ET and R_{ECO} . Remotely sensed data ~~are~~can be good proxies for plant productivity and can be easily implemented into machine-learning models for ET and R_{ECO} estimation, such as for an enhanced vegetation index, land surface water index and ~~NDVI~~normalized differences vegetation index (NDVI) (Gao et al., 2015; Jägermeyr et al., 2014; Migliavacca et al., 2015). Li and Xiao (2019) developed a data-driven model ~~for~~to estimate gross primary production at a spatial and temporal resolution of 0.05° and 8 days, respectively, using MODIS and meteorological reanalysis data. Berryman et al. (2018) demonstrated the value of a Random Forest model to predict growing season soil respiration from subalpine forests in the Southern Rocky Mountains ecoregion. Jung et al. (2009) developed a model tree ensemble approach to upscale FLUXNET data, where they ~~have~~successfully estimated ET and GPP. Other methods have used support vector machines, artificial neural networks, random forest, and piecewise regression (Bodesheim et al., 2018; Metzger et al., 2013; Xiao et al., 2014; Xu et al., 2018). These models were trained with ground-measured flux observations and other variables, and then applied to estimate ET over continental or global scales with remote sensing and meteorological inputs. Some of the most important inputs include the enhanced vegetation index, aridity index, temperature, and precipitation. However, the spatiotemporal resolution of these approaches is constrained by the resolution of remote sensing products and meteorological inputs. Additionally, parameters such as leaf area index, cloudiness, and the vegetation types required by those models may not be available at the required resolution, accuracy or location. For example, in systems that have significant elevation gradients, errors may result when valley-based FLUXNET data are used for training and then applied to hillslope or ridge ET and R_{ECO} estimation.

Development of hybrid models that link direct measurements and/or interpretable mechanistic models with data-driven methods can benefit ET and R_{ECO} estimation (Reichstein et al., 2019). While remote sensing data that cover large regions provide promise for informing models, quantitative interpretation of these data needed for input into mechanistic models is still challenging (Reichstein et al., 2019). Physically-based models can provide estimates of ET and R_{ECO} , but the estimate error can be high, owing to parametric, structural, and conceptual uncertainties as described above. Hybrid data-driven frameworks are potentially advantageous because they enable the integration of remote sensing datasets, meteorological forcings, and mechanistic model outputs of ET and R_{ECO} into one model. Machine-learning approaches are then applied to extract the spatiotemporal patterns for ET and R_{ECO} prediction. Hybrid models can utilize the high spatial coverage of remote sensing data (e.g., 30 m of Landsat) and high temporal

resolution of direct measurement from flux towers or simulation results from mechanistic models (e.g., daily or hourly scales), thus providing alternative approaches for next-stage, more accurate estimation of ET and R_{ECO} at greater spatial and finer temporal scales—and enhancing our process understanding of water and carbon cycling under climate change.

In this study, we developed a hybrid predictive modeling approach (HPM) to better estimate daily ET and R_{ECO} ~~over space and time~~ with easily acquired meteorological data (i.e., air temperature, precipitation and radiation) and remote sensing products (i.e., NDVI). HPM is hybrid as it can use deep learning models to integrate direct measurements from flux towers and physically-based model results (e.g., CLM) with meteorological and remote sensing inputs to capture the complex physical interactions within the watershed ecosystem. After development, we validated HPM performance with the FLUXNET dataset and benchmarked the CLM model at select sites. We then used the HPM for ET and R_{ECO} estimation at the mountainous East River Watershed in ~~CO~~Colorado, USA and investigated how ~~small-scale heterogeneity influences~~ ET and R_{ECO} dynamics ~~-~~ varies within the East River Watershed.

The remainder of this paper is organized as follows. Section 2 mainly describes the sites considered in this study and how data were acquired and processed. Section 3 presents the methodology of the HPM approach, followed by the results of various use cases presented in Section 4. Discussion and conclusion are provided in Sections 5 and 6, respectively.

2. Site Information, Data Acquisition and Processing

~~———— We selected various sites to develop and validate our approaches. We focused on mountainous watersheds because they provide significant water resources to the world (Viviroli et al., 2007), but also included sites to test HPM's capabilities under different climate and vegetation conditions. Mountainous watersheds are very sensitive to changes in temperature and precipitation patterns, which can significantly threaten downgradient water resources and associated societal benefits (Breshears et al., 2005; Ernakovich et al., 2014; Immerzeel et al., 2019). As mountainous regions are extremely important for regional and global assessment and management of water resources and carbon storage and emission (Knowles et al., 2015; Schimel et al., 2002), accurate estimation of ET and R_{ECO} in these regions is critical, though challenging due to complex heterogeneity and complicated interactions among the hydrosphere, biosphere and the atmosphere (Pelletier et al., 2018; Speckman et al., 2015). Thus, we focused on estimating ET and R_{ECO} at various sites along the Rocky Mountains, including the East River Watershed (Hubbard et al., 2018) of the Upper Colorado River Basin.~~

~~———— The HPM method was tested using data from a range of different ecosystem types to explore its performance under different conditions. However, we place a particular focus on mountainous sites, given their regional and global importance yet challenges associated with ET and R_{ECO} as described above.~~

2.1 FLUXNET Stations and Ecoregions

~~Eight~~Nine FLUXNET stations were selected for this study (Table 1 and Figure 1), which cover a wide range of climate and ~~vegetation types~~elevations. These stations have elevations from 129 m (US-Var) to 3050 m (US-NR1),

mean annual air temperature from ~~1.5°C (US-NR1)~~ 0.34°C (CA-Oas) to 17.92 °C (US-SRM), and mean annual precipitation from 320 mm (US-Whs) to 800 mm (US-NR1). These FLUXNET stations also cover a wide range of vegetation types (i.e., evergreen forest, deciduous forest, and shrublands). As indicated by Hargrove et al. (2003), FLUXNET stations provide a good representation of different ecoregions, which are areas that display recurring patterns of similar combinations of soil, vegetation and landform characteristics (Omernik, 2004). Omernik & Griffith. (2014) delineated the boundaries of ecoregions through pattern analysis that consider the spatial correlation of both physical and biological factors (i.e., soils, physiography, vegetation, land use, geology and hydrology) in a hierarchical level. FLUXNET stations considered in this study mainly locate in 4 unique ecoregions (Table 1). As is described below, we developed local-scale (i.e., point scale) HPM that are representative for different ecoregions using data provided at these FLUXNET stations to estimate ET and R_{ECO} , and validated the HPM estimates with measurements from stations within the same ecoregion.

2.2 SNOTEL Stations

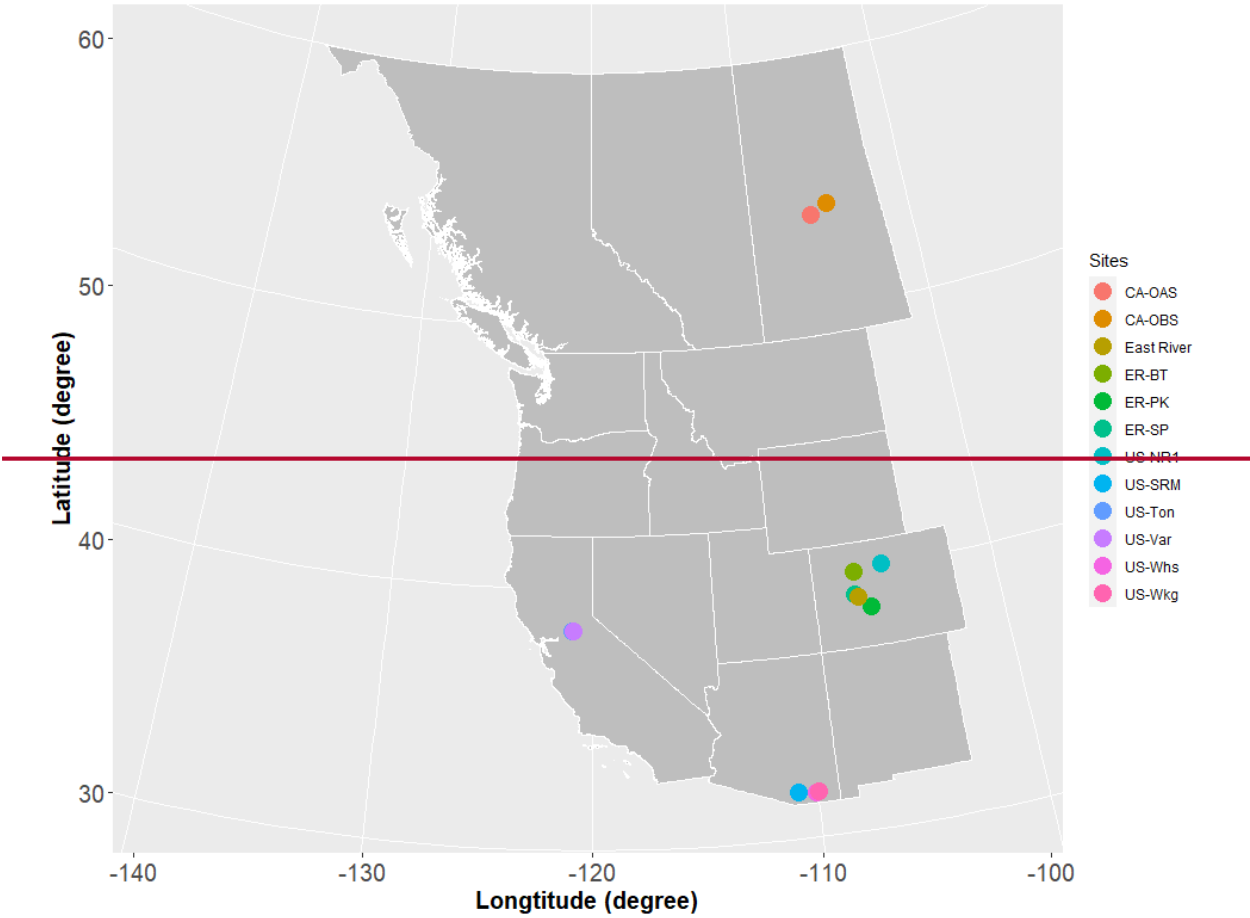
For reasons described below, we performed a deeper exploration of HPM performance within one of the mountainous watershed sites (the East River Watershed of the Upper Colorado River Basin), which is located in the “western cordillera” ecoregion. At this site, we utilized meteorological forcings data from three snow telemetry (SNOTEL) stations. These sites include the Butte (ER-BT, id: 380), Porphyry Creek (ER-PK, id: 701) and Schofield Pass (ER-SP, id: 737) sites. A CLM model was developed at these SNOTEL stations that provides physically-model-based ET estimation (Tran et al., 2019). Table 1 summarizes the SNOTEL stations used in this study and the corresponding climate characteristics. Figure 1 shows the geographical locations of FLUXNET and SNOTEL stations selected in this study.

Table 1. Summary of FLUXNET stations and SNOTEL stations information. * denotes SNOTEL stations and all others are FLUXNET stations. Dfc, Bsk, Csa represent subarctic or boreal climates, semi-arid climate, Mediterranean hot summer climates, respectively. ENF, DBF, WSA, GRA, and OSH represent evergreen needleleaf forest, deciduous broadleaf forests, woody savannas, grasslands, open shrubland, respectively. FLUXNET data were obtained from the FLUXNET2015 database.

Site ID	Site Name	Latitude, Longitude	Elevation (m)	Mean Annual temperature (°C)	Mean Annual Precipitation (m)	Climate Koeppen	Vegetation IGBP	Ecoregions (Level II)	Period of Record
US-NR1	Niwot Ridge	(40.0329, -105.5464)	3050	1.5	800	Dfc	ENF	Western Cordillera	2000-2014
CA-Oas	Saskatchewan-Aspen	(53.6289, -106.1978)	530	0.34	428.53	Dfc	DBF	Boreal Plain	1997-2010
CA-Obs	Saskatchewan-Black Spruce	(53.9872, -105.1178)	628.94	0.79	405.6	Dfc	ENF	Boreal Plain	1999-2010
US-SRM	Santa Rita Mesquite	(31.8214, -110.8661)	1120	17.92	380	Bsk	WSA	Western Sierra Madre Piedmont	2005-2015
US-Ton	Tonzi Ranch	(38.4316, -120.9660)	177	15.8	559	Csa	WSA	Mediterranean California	2002-2015
US-Var	Vaira Ranch-lone	(38.4133, -120.9507)	129	15.8	559	Csa	GRA	Mediterranean California	2002-2015
US-Whs	Walnut Gulch Lucky Hills Shrub	(31.7438, -110.0522)	1370	17.6	320	Bsk	OSH	Western Sierra Madre Piedmont	2008-2015

US-Wkg	Walnut Gulch Kendall Grasslands	(31.7365, -109.9419)	1531	15.64	407	Bsk	GRA	Western Sierra Madre Piedmont	2005-2015
<u>US-Me2</u>	<u>Metolius mature ponderosa pine</u>	<u>(44.4523, -121.5574)</u>	<u>1253</u>	<u>6.28</u>	<u>523</u>	<u>Csb</u>	<u>ENF</u>	<u>Western Cordillera</u>	<u>2012-2015</u>
ER-BT*	East River-Butte	(38.894, -106.945)	3096	2.38	821	Dfc	N/A	Western Cordillera	1995-2017
ER-SP*	East River-Schofield Pass	(39.02, -107.05)	3261	2.46	1064	Dfc	N/A	Western Cordillera	1995-2017
ER-PK*	East River-Porphry Creek	(38.49, -106.34)	3280	1.97	574	Dfc	N/A	Western Cordillera	1995-2017

206



207

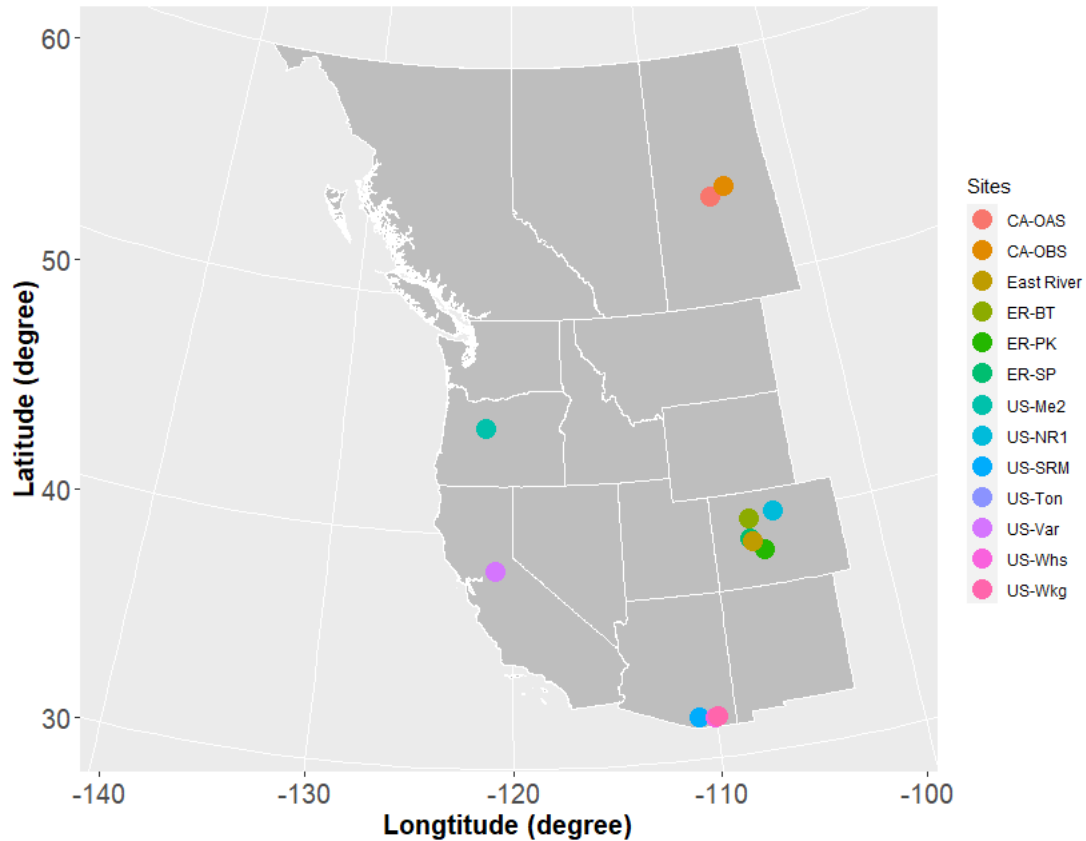


Figure 1. Location of sites considered in this study. Note: US-Ton and US-Var; US-Whs and US-Wkg are at the same locations. East River Watershed is located next to ER-BT. The white lines delineate Western US states and Canadian provinces.

2.3 East River Watershed and Previous Analyses

Data from the East River Watershed were used to explore how ET and R_{ECO} dynamics estimated from the developed HPM vary with different vegetation and meteorological forcings. The East River Watershed is located northeast of the town of Crested Butte, Colorado. This watershed has an average elevation of 3266 m, with significant gradients in topography, hydrology, geomorphology, vegetation, and weather. The watershed has a mean annual temperature around 0°C, with an average of 1200 mm yr⁻¹ total precipitation (Hubbard et al., 2018). Consisting of montane, subalpine, and alpine life zones, each with distinctive vegetation biodiversity, the East River Watershed is a testbed for the US Department of Energy Watershed Function Scientific Focus Area Project, led by the Lawrence Berkeley National Laboratory (LBNL; Hubbard et al., 2018). The project has acquired a range of datasets, including hydrological, biogeochemical, remote sensing, and geophysical datasets.

Recently completed studies at the East River Watershed were used in this study to inform HPM and to assess the results. For example, physically-model-based estimations of ET at this site (Tran et al., 2019) were used herein for HPM development and validation. ~~Falco et al. (2019) used machine learning based remote sensing methods to characterize the spatial distribution of vegetation types, slopes, and aspects within a hillslope at the East River~~

Watershed, which were used with obtained HPM estimates to explore how small scale vegetation heterogeneity influences ET and R_{ECO} dynamics. To perform this assessment, we computed the spatial distribution of vegetation types at watershed scale, based on Falco et al. (2019), and selected 16 locations within the East River Watershed having different vegetation types and slope aspects. These 16 locations were chosen at a level to be distinguishable by Landsat images and maintain the same vegetation type (given a spatial resolution of 30 m), and also possess small-scale heterogeneity. Falco et al. (2019) used machine-learning-based remote sensing methods to characterize the spatial distribution of vegetation types, slopes, and aspects within a hillslope at the East River Watershed, which were used with obtained HPM estimates to explore how vegetation heterogeneity influences ET and R_{ECO} dynamics. To perform this assessment, we computed the spatial distribution of vegetation types at watershed scale based on Falco et al. (2019). We evaluated manually and selected 16 locations within the East River Watershed having different vegetation types and slope aspects. These 16 locations were chosen to be at the center of vegetation patched and covered by one vegetation type. A summary of the locations is presented in Table 2; the spatial distribution of the locations is shown in Figure 2.

Table 2: Location and vegetation types of East River Watershed sampling points (Figure 2)

Easting (m)	Northing (m)	Vegetation Type	Aspect	Elevation (m)
327085	4309878	Deciduous Forest	South	2983
326288	4312504	Deciduous Forest	South	3177
330012	4313132	Deciduous Forest	North	3108
326854	4313192	Deciduous Forest	South	3098
328246	4312832	Meadow	South	3095
327010	4315059	Meadow	South	2790
328738	4306139	Meadow	North	2890
334270	4309465	Meadow	North	2929
333406.5	4308340	Riparian Shrubland	South	2760
327846	4312497	Riparian Shrubland	South	2723
334641	4305632	Riparian Shrubland	North	2740
330760	4310097	Riparian Shrubland	South	2855
329573	4314569	Evergreen Forest	South	3026
333106	4307313	Evergreen Forest	North	3102
325056	4310456	Evergreen Forest	South	2961
335141	4309614	Evergreen Forest	North	3131

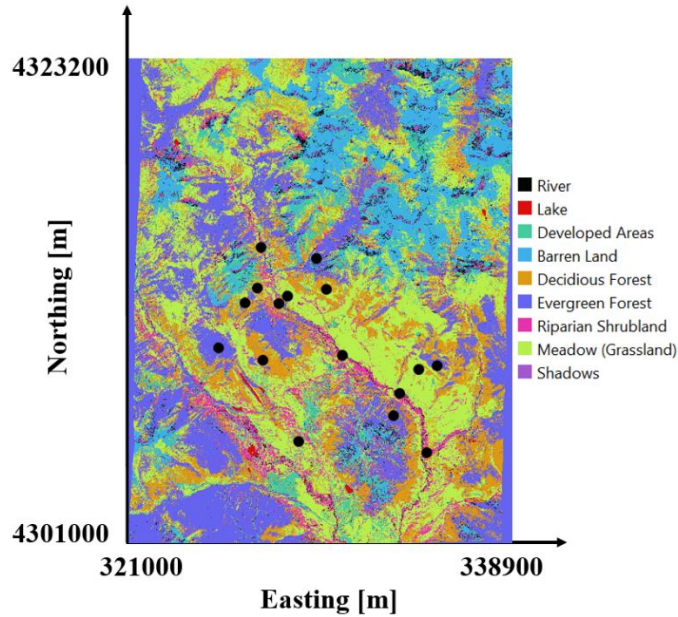


Figure 2: Vegetation classification of the East River, CO Watershed from ~~Falco et al. (2019)~~Falco et al. (2019). East River sites selected in this study are denoted by black circles.

2.4 Data Collection and Processing

To enhance transferability of the developed HPM strategy to less intensively characterized watersheds, we selected only “easy to measure” or “widely available” attributes, such as precipitation, temperature, radiation and NDVI, as inputs to the HTM model. The data sources used for these inputs include FLUXNET data (<https://fluxnet.fluxdata.org/>), SNOTEL data (<https://www.wcc.nrcs.usda.gov/snow/>) and developed CLM model (Tran et al., 2019) at SNOTEL stations, DAYMET meteorological inputs (Thornton et al., 2017) and remote sensing data from Landsat imagery (Irons et al., 2012).

A variety of measured data and model outputs were used to train and validate HPM. We obtained daily meteorological data, including air temperature, precipitation, radiation, ET, and R_{ECO} data, from the FLUXNET database at the selected FLUXNET sites. The pipeline of data processing for FLUXNET dataset is provided at <https://FLUXNET.fluxdata.org/>. We identified some data gaps and erroneous data (especially during winter seasons) for the ET estimates at US-NR1, which were cleaned following the procedures presented in Rungee et al. (2019). The meteorological data were used as inputs for HPM development, and ET and R_{ECO} data from these sites were used for HPM validation. At the three selected SNOTEL stations, we obtained air temperature, precipitation, and snow-water-equivalent data from the SNOTEL database. Air temperature data at these three SNOTEL stations were processed following Oyler et al. (2015), given potential systematic artifacts. Snow-water-equivalent data are not easily acquired, and thus were not considered as inputs for HPM. However, a categorical variable was constructed to assimilate information regarding snow (Section 3.2.1). CLM models were generated following Tran et al. (2019) for the SNOTEL stations and US-NR1 to assess the spatiotemporal variability of ET at the East River Watershed and for training and validating HPM (Section 4.3). The DAYMET dataset (Thornton et al., 2017) provided gridded daily

weather-forcings-attribute estimates at a 1 km spatial resolution. We obtained the incident radiation data from DAYMET at the SNOTEL stations as inputs for HPM. For the East River Watershed sites, meteorological forcings data, including air temperature, precipitation and radiation, were also obtained from DAYMET. The low spatial resolution of DAYMET data introduces uncertainty in HPM estimation of ET and R_{ECO} , which will be discussed in the following sections. We calculated the NDVI time series from the red band (RED) and near-infrared band (NIR) from Landsat 5, 7, and 8 images following Equation 1 at all selected FLUXNET sites, SNOTEL stations, and East River Watershed sites at a spatial scale of 30 m.

$$NDVI = \frac{NIR - RED}{NIR + RED} \quad (1)$$

Since cloud conditions can severely decrease data quality, we used the cloud-scoring algorithm provided in the Google Earth Engine to mask clouds in all retrieved data, only selecting the ones that had a simple cloud score below 20 to ensure data quality. Given the different calibration sensors used in Landsat 5, 7, and 8, we also followed the processes described in Homer et al. (2015) and Vogelmann et al. (2001) to keep NDVI computations consistent over time. Landsat satellites have a return period of 16 days, and thus we performed a reconstruction of NDVI time series to obtain daily scale time data (Section 3.2.2).

3. Hybrid Predictive Modeling Framework

In this section, we illustrate the steps for building an HPM model for ET and R_{ECO} estimation over time and space. Figure 3 presents the general framework of HPM, which includes modules for data preprocessing, model development, model validation, and predictive modeling.

3.1 Model Framework

HPM establishes relationships among meteorological forcings attributes, NDVI, ET, and R_{ECO} (Figure 3). Both input data (e.g., meteorological forcings) and output data (ET and R_{ECO}) used for training and validation are preprocessed for gap filling, smoothing, and data updating. HPM “learns” the complex space-time relationship among meteorological forcings, NDVI, ET, and R_{ECO} using a deep-learning-based module (deeply connected neural networks and a long short-term memory recurrent neural network). HPM then can be used for ET and R_{ECO} estimation at sparsely monitored watersheds. Individual HPM models can be trained in two different ways using ET and R_{ECO} information: with data obtained from flux towers (“data-driven HPM”) or with outputs from 1-D physically-based models (“mechanistic HPM”). In both cases, the models obtained with local data are then used to estimate ET and R_{ECO} at other sites in the same ecoregion (see Section 2.1). For ecoregions not represented by FLUXNET sites, it is necessary to develop mechanistic HPM that enables ET and R_{ECO} estimation over space and time.

HPM has several additional modules, including model development, model validation, and model prediction modules. In the HPM model development module, deep-learning algorithms are trained with input features and response data until a pre-defined “stopping criteria” (e.g., root mean squared error, RMSE) is met, indicating subsequent training would lead to minimal improvement. In the validation module, estimation outputs from the

“trained HPM models” are compared with other ET and R_{ECO} data obtained from other independent sites or mechanistic models within the same ecoregion. Statistical measures, including adjusted R^2 and mean absolute error (MAE), are computed to evaluate the performance of HPM models. In the predictive model module, meteorological forcings data and remote sensing data are processed at target sites of interest, and the validated HPM model is used to estimate ET and R_{ECO} at these sites. ET and R_{ECO} outputs estimated from HPM at sparsely monitored watersheds then provide alternative datasets for process understanding within the target watersheds.

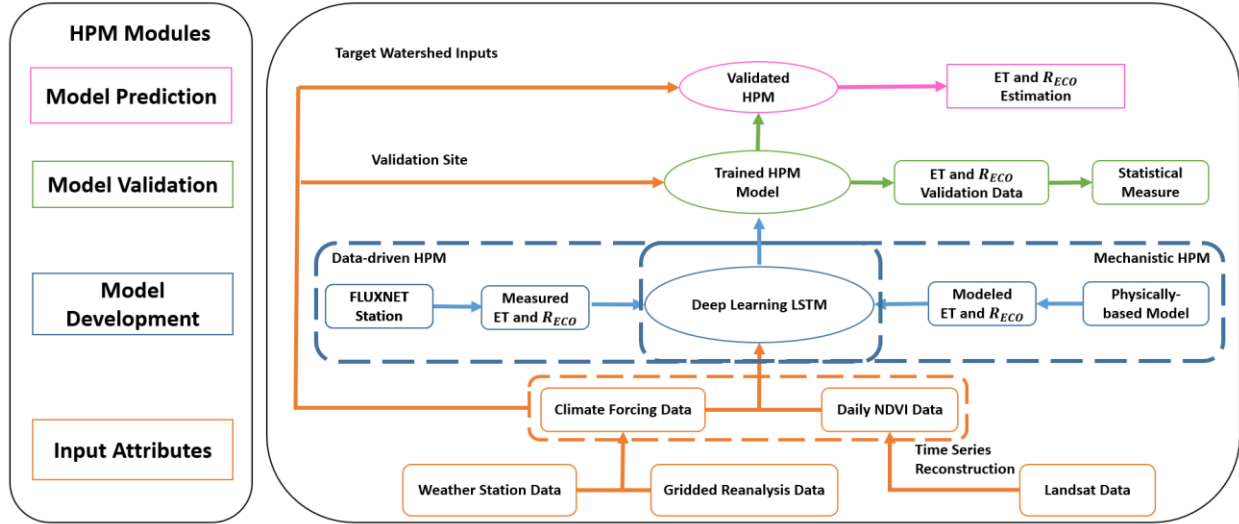


Figure 3: Hybrid Predictive Model (HPM) Framework. The HPM model mainly consists of four modules: Input Attributes, Model Development, Model Validation and Model Prediction, represented by rectangles with colors. Arrows represent the linkages among different modules. Choices of data-driven HPM or mechanistic HPM depend on the ecoregion of target watershed and data availability.

Long short-term memory (LSTM, Hochreiter & Schmidhuber, 1997) is capable of identifying long-term dependencies between climate and environmental data. For example, Kratzert et al. (2018) successfully used LSTM to learn the long-term dependencies in hydrological data (e.g., storage effects within catchments, time lags between precipitation inputs and runoff generation) for rainfall-runoff modeling. LSTM has also been used for gap filling in hydrological monitoring networks in the spatiotemporal domain (Ren et al., 2019). In this study, the outputs (ET or R_{ECO}) denoted as y are predicted from the input $x = [x_1, x_2, \dots, x_T]$, consisting of the last T consecutive time steps of attributes, such as meteorological forcings attributes (e.g., air temperature and precipitation) and remote sensing attributes (i.e., NDVI). In a recurrent neural network (RNN), h_t represents the internal state at every time step t that takes in current input value x_t and previous internal state h_{t-1} , and is recomputed along the time axis using the following equation:

$$h_t = g(Wx_t + Uh_{t-1} + b), \quad (21)$$

where g represents the hyperbolic tangent activation function, W and U are trainable weight metrics of the hidden state h , and b is a bias vector. W , U and b are all trainable through optimization. LSTM introduces the cell state c_t ,

which makes LSTM powerful in identifying long-term dependencies in a statistical manner. The cell state c_t has three gates structures, including “forget gates” (which determine what information from previous cell states will be forgotten), “input gates” (which determine what information will be conveyed from the forget gate) and “output gates” (which return information from cell state c_t to a new state h_t). With these gate structures, the cell state c_t controls what information will be forgotten, conveyed, and updated over time. The forget gate is formulated as follows:

$$f_t = \sigma(W_f x_t + U_f h_{t-1} + b_f), \quad (32)$$

where f_t results in a value between 0 and 1 indicating the degree of information to be forgotten; σ is the logistic sigmoid function, and W_f, U_f and b_f are trainable parameters. Next, the input gate decides which values will be updated in the current cell state, and creates a vector of candidate values \tilde{c}_t in the range of (-1, 1) through a \tanh layer, which will be used to update the current state. With the candidate values calculated from the current state, and the information conveyed from the forget gate, we can calculate the current cell state as follows:

$$i_t = \sigma(W_i x_t + U_i h_{t-1} + b_i), \quad (43)$$

$$\tilde{c}_t = \tanh(W_{\tilde{c}} x_t + U_{\tilde{c}} h_{t-1} + b_{\tilde{c}}), \quad (54)$$

$$c_t = f_t * c_{t-1} + i_t * \tilde{c}_t, \quad (65)$$

where i_t is the input gate that defines which information of \tilde{c}_t will be used to update the current cell state and is in the range of (0, 1); c_t represents the current cell state; and $W_{\tilde{c}}, U_{\tilde{c}}, b_{\tilde{c}}, W_i, U_i$, and b_i are trainable parameters. Finally, the output gate o_t controls the information of cell state c_t to a new hidden state h_t , which is computed using the following equation:

$$o_t = \sigma(W_o x_t + U_o h_{t-1} + b_o), \quad (76)$$

$$h_t = \tanh(c_t) * o_t, \quad (87)$$

With the new hidden state calculated, ET and R_{ECO} can be calculated using a one unit dense layer:

$$y_t = W_d h_t + b_d, \quad (98)$$

where W_d and b_d are additional trainable parameters. In summary, the LSTM unit calculates the internal state using current meteorological forcings and remote sensing data at every time step. The forget gate, input gate, and output gate decide what information from previous time steps will be kept, updated, and conveyed to the new hidden state. Finally, with a single dense layer, the algorithm will output ET and R_{ECO} estimation from the trained model.

A 70%-30% split between training and validation time series data was applied here, where the first 70% of the data were used for HPM development as a learning process, and 30% of the data were used as validation sets at individual sites. At the East River Watershed, HPM results were also validated with benchmark CLM outputs from Tran et al. (2019) and FLUXNET measurements. We used the mean absolute error (MAE), and adjusted R^2 as the statistical measure to determine model performance.

$$MAE = \frac{\sum_{i=1}^n |y_{predict} - y_{measured}|}{n}, \quad (10)$$

$$R^2 = 1 - \frac{SSE}{SS}, \quad (11)$$

where SSE represents the sum of squared errors, SS is the sum of squares of the response attributes (i.e., ET or R_{ECO}), and n is the number of data points. In most models, the configuration of the neural networks includes a first LSTM layer with 50 units, a second LSTM layer with 25 units, and a dense layer with 8 units having L2 regularizers and a final output dense layer. Dropout layers are also embedded in the model to prevent overfitting. There are 11600 and 7600 parameters for the first and second LSTM layers; 208 and 9 for the first and second dense layers and no parameters for the dropout layers. Other configurations of networks may provide better estimation results; however, they are not assessed in this study, as the proposed configuration already provide reasonable results. More information about the LSTM-RNN method is provided by (Olah, 2015)Olah. (2015).

3.2 Feature Selection

Given data availability and the practicability of applying HPM to estimate ET and R_{ECO} at sparsely monitored watersheds, we also selected, constructed, and augmented certain attributes as features for HPM. Key properties influencing ET and R_{ECO} dynamics are linked to snow processes, plant dynamics, moisture stresses, radiation inputs and other relevant processes. However, at sparsely monitored watersheds, only weather reanalysis data and remote sensing data are commonly available. Thus we mainly considered temperature, radiation, precipitation, vegetation indices (e.g., NDVI) and variables inferred from these data as inputs for HPM. Other key attributes that depend on depth and site specific characteristics such as soil moisture and snow depth are not used in current HPM models due to data availability.

3.2.1 Snow information

In mountainous watersheds, snow dynamics significantly influence water and carbon fluxes. Because of the difficulties in measuring snow time series over space, we did not directly use attributes such as snow water equivalent as input to HPM. Instead, we separated precipitation data into snow precipitation (air temperature < 0) and rainfall precipitation (air temperature > 0). This is in line with what has been used in hydrological models such as CLM (Oleson et al., 2013). Note that for certain sites in this study, snow is not present (e.g., US-Ton). In order to capture the dynamics of snow processes, such as accumulation and melting, we constructed a categorical variable (sn), as follows:

$$sn = \begin{cases} 0, & \text{during snow accumulation; } SWE > 0 \text{ and } SWE < \text{peak } SWE \\ 1, & \text{during snow melting; } SWE > 0 \text{ and } SWE \leq \text{peak } SWE \\ 2, & \text{no snow; } SWE = 0 \end{cases}, \quad (129)$$

Since data on peak SWE are rarely available because of the difficulties in measuring snow, we also define a proxy categorical variable, *sn*. When no SWE measurements were available, we estimated *sn* using air and soil temperature data following Knowles et al. (2016), who found significant correlations between the day of peak snow accumulation and first day of air temperature above 0 degrees Celsius, as follows:

$$sn = \begin{cases} 0, & \text{during snow accumulation; Air Temperature} < 0 \\ 1, & \text{during snow melting; Air Temperature} > 0 \text{ while Soil Temperature} \leq 0, \\ 2, & \text{no snow; Air Temperature and Soil Temperature} > 0 \end{cases} \quad (1310)$$

3.2.2 Vegetation information

To mitigate the long return periods of satellites and the presence of clouds, we reconstructed daily NDVI values based on meteorological forcings data (e.g., air temperature, precipitation, radiation) using deep-learning recurrent neural networks, leading to estimates of NDVI at daily temporal resolution. For example, Figure 4 represents Landsat-derived NDVI and reconstructed NDVI values for two sites at the East River, CO watershed: Butte (ER-BT), and Schofield Pass (ER-SP). Figure 4 reveals that based on meteorological forcings data only, the reconstructions achieved an adjusted R^2 of 0.65. Though not ideal, as satellites continue to advance and more training data becomes available, the accuracy of NDVI temporal reconstruction willis expected to increase.

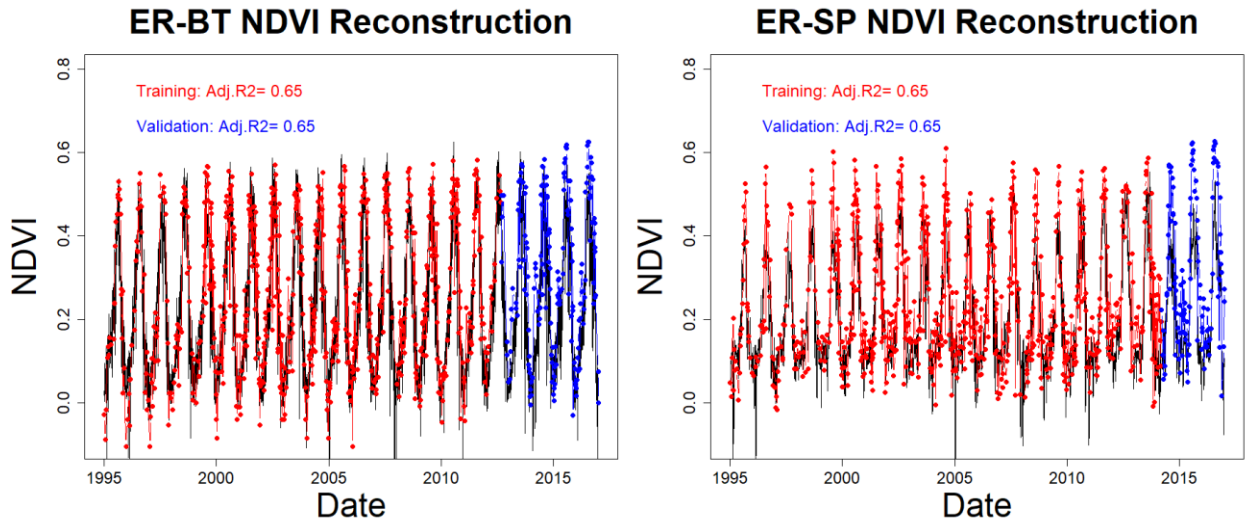


Figure 4: Temporal reconstruction of NDVI at ER-BT (left) and ER-SP (right). Black ~~line represents~~ lines represent reconstructed daily NDVI. Red points are used for training and blue points are used for validation

4. Results

We tested HPM's capabilities using four different use cases to explore different conditions. First, we tested the capability of HPM to estimate long-term temporal dependency among meteorological forcings, ET, and R_{ECO} (Use Case 1; presented in Section 4.1). Second, we validated HPM's capability to estimate the spatial distribution of ET and R_{ECO} over space in selected watersheds, where we developed HPM using existing FLUXNET data (Use Case 2; data-driven HPM, Section 4.2) or outputs from a mechanistic model (Use Case 3; physical-model-based HPM, Section 4.3). ~~Third~~In Use Case 4, HPM was used to estimate ET and R_{ECO} at selected sites within the East River Watershed and to distinguish how ~~local factors (e.g., vegetation heterogeneity) influence~~ ET and R_{ECO} dynamics varies in the East River Watershed (Section 4.4). Temporal resolution of HPM models for all Use Cases are at daily scale and the spatial resolution depends on the use of meteorological forcing data. These four use cases illustrate and demonstrate how HPM can be developed and applied at target watersheds; where data are sparse.

4.1 Use Case 1: ET and R_{ECO} Time Series Estimation with HPM Developed at FLUXNET Sites

Local HPMs were developed to estimate ET and R_{ECO} using flux tower data obtained from FLUXNET sites listed in Table 1. ~~Attributes~~At all FLUXNET sites, air temperature, precipitation, net radiation, NDVI and soil temperature were used to train these individual HPM are documented in Table 3.

Table 3. Attributes used for HPM development in Use Case 1

Site ID	Site Name	Attributes
US-NR1	Niwot Ridge	Air Temperature, precipitation, net radiation, sn, NDVI, soil temperature
CA-Oas	Saskatchewan-Aspen	Air Temperature, precipitation, net radiation, sn, NDVI, soil temperature
CA-Obs	Saskatchewan-Black Spruce	Air Temperature, precipitation, net radiation, sn, NDVI, soil temperature
US-SRM	Santa Rita Mesquite	Air Temperature, precipitation, net radiation, NDVI, soil temperature
US-Ton	Tonzi Ranch	Air Temperature, precipitation, net radiation, NDVI, soil temperature
US-Var	Vaira Ranch-lone	Air Temperature, precipitation, net radiation, NDVI, soil temperature
US-Whs	Walnut Gulch-Lucky Hills Shrub	Air Temperature, precipitation, net radiation, NDVI, soil temperature
US-Wkg	Walnut Gulch-Kendall Grasslands	Air Temperature, precipitation, net radiation, NDVI, soil temperature

. For US-NR1, CA-Oas and CA-Obs, sn is also included. The results, which are shown in Figure 5 and Table 43, reveal that the HPM approach was effective for estimating ET. Adjusted R^2 between the ~~HTM~~HPM estimates and flux tower measurements are above 0.85 for all sites, and mean absolute errors are small at a level of $\sim 0.2 \text{ mm/d}$. Figure 5 displays the daily scale estimation of ET from HPM US-NR1 and CA-OAS (other sites provided in supplementary material), and presents monthly mean ET values of measurements, HPM estimations, and differences. The long-term trends in ET are well captured by HPM. At larger temporal scales (monthly or yearly), HPM provides reasonable estimation of ET at these sites. However, short-term fluctuations during the summer are also not well captured by ET, specifically at California sites during the periods when plant transpiration and soil evaporation are constrained by soil moisture (Figure A2 panel a).

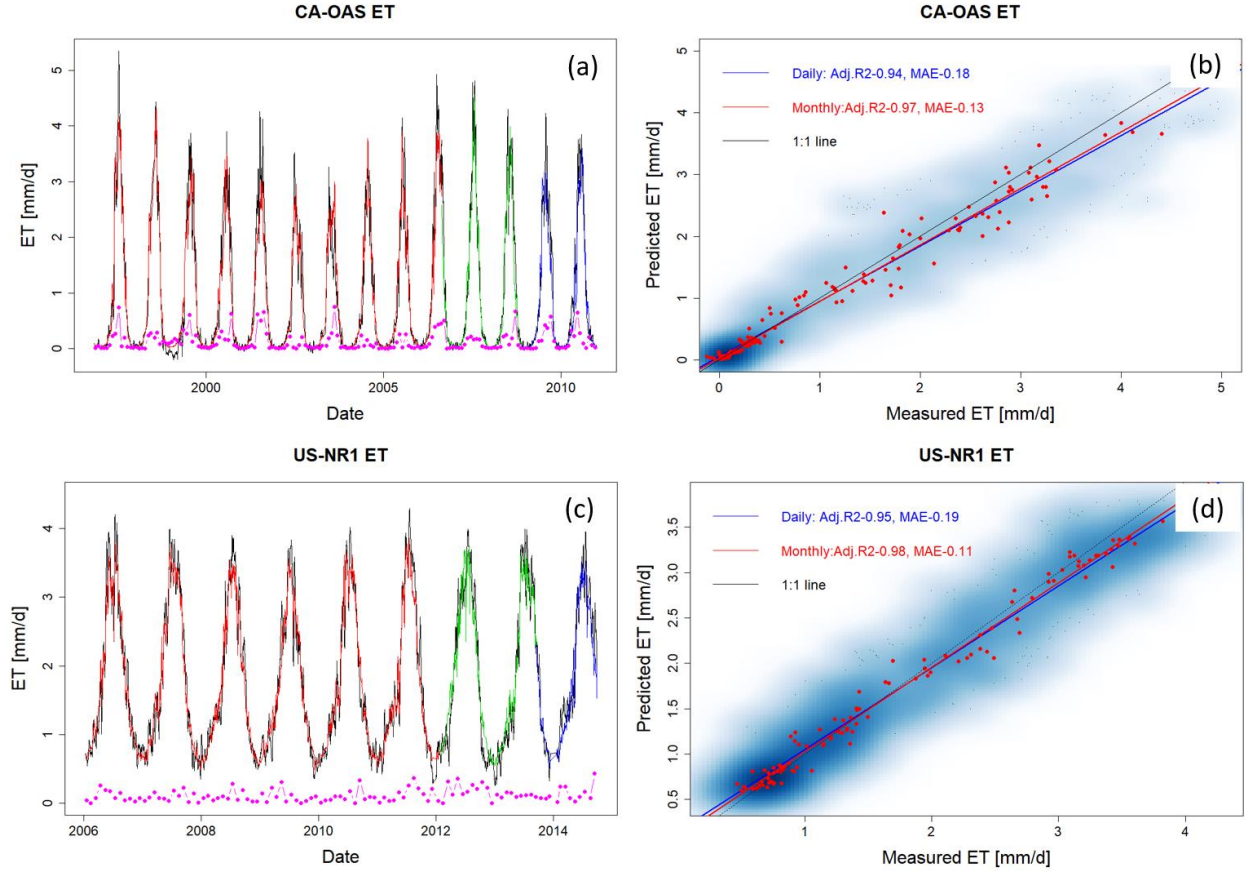


Figure 5: ET estimation with data from FLUXNET sites at CA-OAS and US-NR1. Panels (a) and (c) illustrate the daily estimation of ET with red, green, and blue lines representing data used for training, validation, and prediction, respectively, and the black line showing the eddy covariance measurements. Pink points describe monthly mean difference between HPM estimation and measured data. Panels (b) and (d) show the scatter plots of daily (blue) and monthly (red) ET. Darker blue clouds represent greater density of data points. Results for other sites are included in supplementary materials below (Figures A1 and A2).

Similarly, Table 43 and Figure 6 reveal that HPM was also effective in estimating R_{ECO} , leading to small MAE and adjusted R^2 of 0.8 between estimated and measured R_{ECO} except for US-Ton and US-Var. Figure 6 presents HPM-estimated R_{ECO} at US-NR1 and CA-OAS, with other sites presented in Figures A3 and A4. Long-term dynamics of R_{ECO} are also successfully captured by HPM; however, HPM ~~underestimates~~ does not accurately capture R_{ECO} during peak growing seasons. For example, we observed an over estimation of R_{ECO} during 2012 summer at US-Whs, ~~whereas~~ at US-NR1, error increased HPM-estimation during the peak growing season, ~~when estimates of R_{ECO} are smaller than measured R_{ECO} values.~~ While soil moisture ~~can limit~~ is important for R_{ECO} during peak growing season (Ng et al., 2014; Wang et al., 2014), the developed HPM currently does not include soil moisture as a key attribute. As such, HPM underestimates R_{ECO} during peak growing season, leading to higher MAE than other times of the year. ~~In addition,~~ HPM R_{ECO} estimation at US-Ton and US-Var show higher uncertainties (i.e., $MAE > 0.4$ and Adj. $R^2 < 0.8$), ~~which also indicates that soil moisture data is necessary to increase R_{ECO} prediction accuracy in this~~

ee region ($R^2 < 0.8$). At these sites limited by water conditions (e.g., US-Ton) and sites with seasonally dry periods (e.g., US-Whs), it is necessary to include variables that could provide information regarding moisture stresses in the subsurface. Soil moisture that directly quantify water stress can be helpful to increase R_{ECO} prediction accuracy (Noormets et al., 2008). Underestimation of peak growing season R_{ECO} can also come from biases within LSTM training, which is strong in capturing long-term temporal trends but less effective in obtaining peak values, and thus lead to increasing prediction errors during growing season compared to other periods of time.

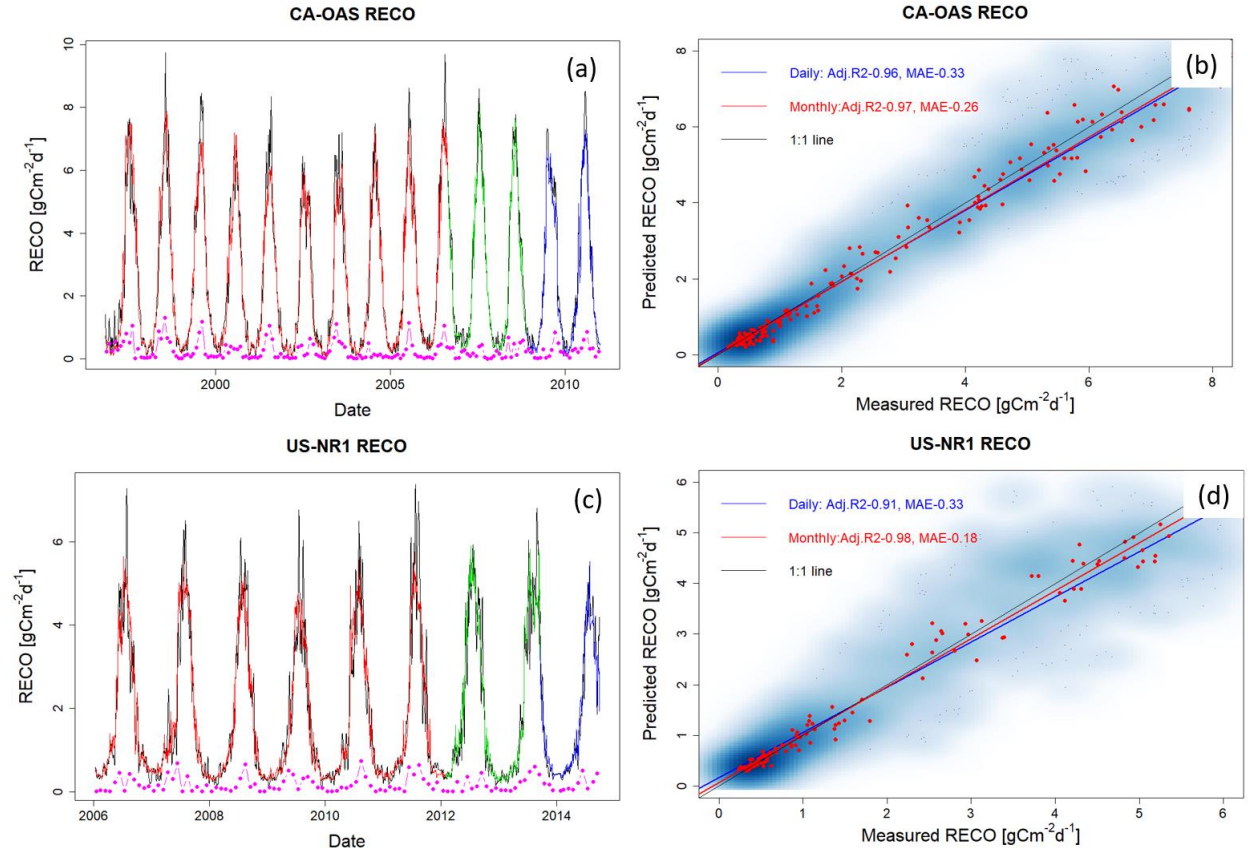


Figure 6: R_{ECO} estimation with data from FLUXNET sites at CA-OAS and US-NR1. Panels (a) and (c) present daily estimation of R_{ECO} with red, green, and blue lines representing data used for training, validation, and prediction, and the black line shows the eddy covariance measurements. Pink points describe monthly mean difference between HPM estimation and measured data. Panels (b) and (d) show the scatter plots of daily (blue) and monthly (red) R_{ECO} . Darker blue clouds represent greater density of data points. Results for other sites are included in supplementary materials below (Figures A3 and A4).

Table 43: Statistical measures of HPM estimation of ET and R_{ECO}

Site ID	Train MAE -ET [mm/d]	Test MAE -ET [mm/d]	Train Adj. R^2 - ET	Test Adj. R^2 - ET	Train MAE - R_{ECO} [$gCm^{-2}d^{-1}$]	Test MAE - R_{ECO} [$gCm^{-2}d^{-1}$]	Train Adj. R^2 - R_{ECO}	Test Adj. R^2 - R_{ECO}
US-NR1	0.19	0.11	0.95	0.98	0.33	0.18	0.91	0.98
CA-Oas	0.18	0.13	0.94	0.97	0.33	0.26	0.96	0.97
CA-Obs	0.12	0.09	0.95	0.96	0.29	0.25	0.96	0.97
US-SRM	0.22	0.17	0.92	0.94	0.24	0.19	0.80	0.87

US-Ton	0.22	0.17	0.92	0.94	0.43	0.36	0.76	0.82
US-Var	0.15	0.12	0.92	0.95	0.49	0.38	0.81	0.88
US-Whs	0.13	0.09	0.93	0.96	0.12	0.09	0.84	0.89
US-Wkg	0.19	0.15	0.87	0.91	0.18	0.15	0.85	0.91

4.2 Use Case 2: Ecoregion-Based, Data-Driven HPM Model for ET and R_{ECO} Estimation

While the effort and cost involved in establishing flux towers naturally limit the spatial coverage of obtained measurements, point scale measurements from one FLUXNET station provides representative information about ecosystem dynamics at other locations within the same ecoregion. In this section, we explored the use of a data-driven HPM trained with one FLUXNET station to estimate ET and R_{ECO} at other locations within the same ecoregion. To test this approach, we first trained HPM at a selected FLUXNET stations and validated these HPM models at other FLUXNET stations (ET and R_{ECO} data at testing sites were only used for comparison with HPM prediction) within the same ecoregion. Specifically, we developed HPM models at US-Ton, CA-Oas and US-Wkg, and provided ET and R_{ECO} estimations at US-Var, CA-Obs and US-Whs at three ecoregions, respectively.

Table 54 summarizes how we developed the data-driven HPM models for spatially distributed estimation of ET and R_{ECO} as well as the corresponding statistical summaries. ~~The estimation led to an adjusted R^2 greater than 0.85 for US-Obs and US-Whs and 0.70 for US-Var.~~ Figures 7 and 8 present the time series of HPM-estimated ET and R_{ECO} compared to measurements from flux towers. ~~The figures HPM estimation at US-Obs, US-Whs and US-Var achieved an adjusted R^2 of 0.87, 0.88 and 0.91 for ET and 0.95, 0.70 and 0.78 for R_{ECO} , respectively. These results show that HPM captures the seasonal and longerlong-term dynamics of ET and R_{ECO} well, as indicated by the high adjusted R^2 .~~ However ~~at sites that experience seasonally dry periods (e.g., US-Whs), prediction accuracy decreases during the peak growing season. For example, we observed an increased errorlarge errors in HPM-based estimations compared to measurements during peak growing seasons (e.g., a 0.5 mm discrepancy in June mean ET). Higher prediction accuracy for~~ We interpret this discrepancy as the ~~two ecoregions presented by US-Whs result that current HPM models did not capture water stress conditions, and CA-Obs are observed compared to US-Ton, which indicates it is necessary to include~~ other key attributes (e.g., soil moisture) ~~are necessary~~ to improve prediction accuracy, especially ~~forat these sites limited by moisture conditions with seasonally dry periods.~~ Although the prediction accuracy is not as high as Use Case 1 (Section 4.1), this use case demonstrates that HPM can learn the complicated relationships between responses and features successfully, and that a local data-driven HPM can be used to fuse with data from other subsites for long-term estimation of ET and R_{ECO} within the same ecoregions.

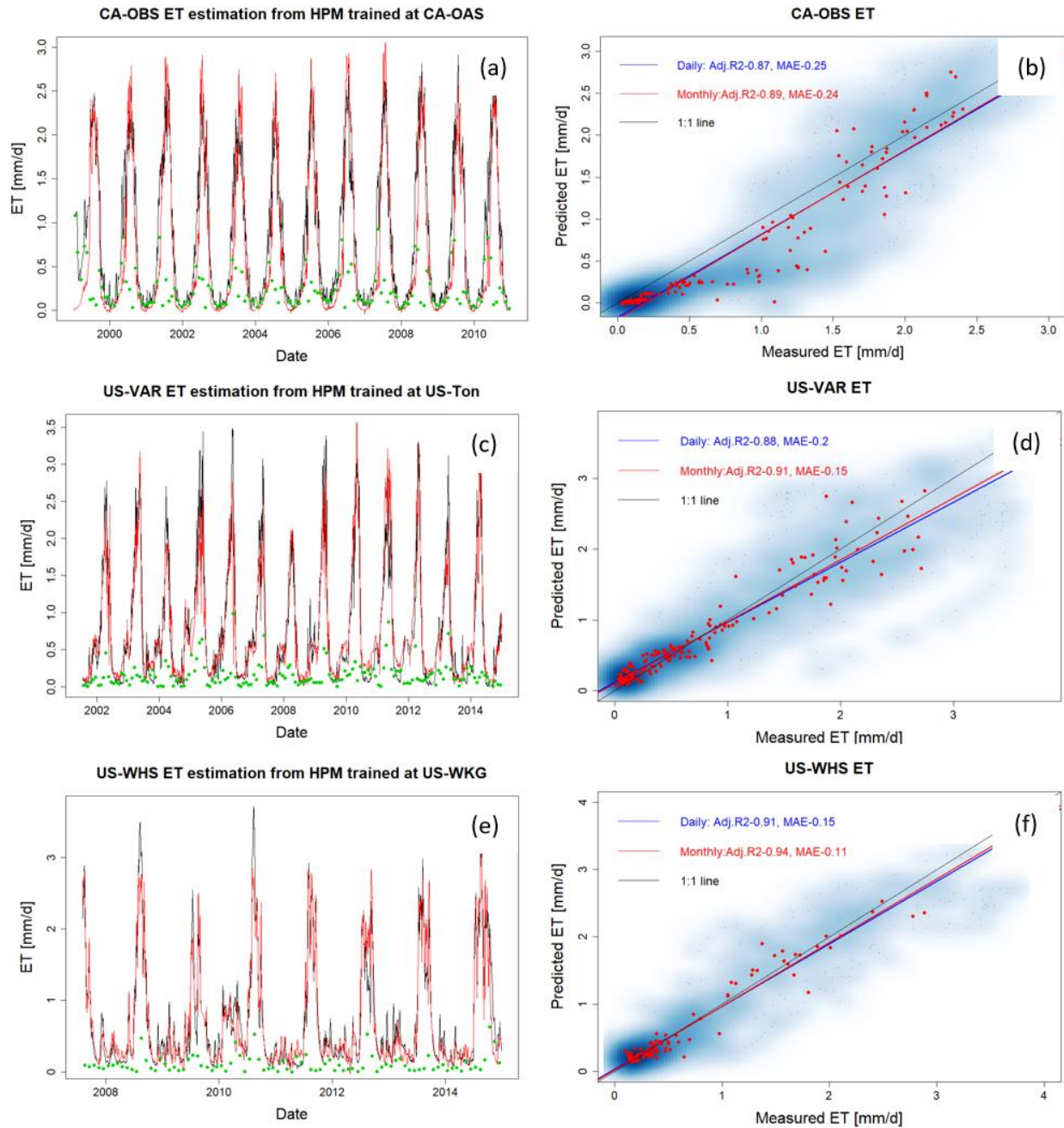


Figure 7. ET estimation at CA-Oas (a), US-Var (c), and US-Whs (e) with HPM trained at US-Ton, US-Wkg, and CA-Oas, respectively. Red and black lines represent HPM estimation and real measurements, with green points denoting the monthly mean difference between HPM estimationss and measurements. Panels (b), (d), and (f) show the scatter plots of daily (blue) and monthly (red) ET at these three sites. Darker blue clouds represent greater density of data points.

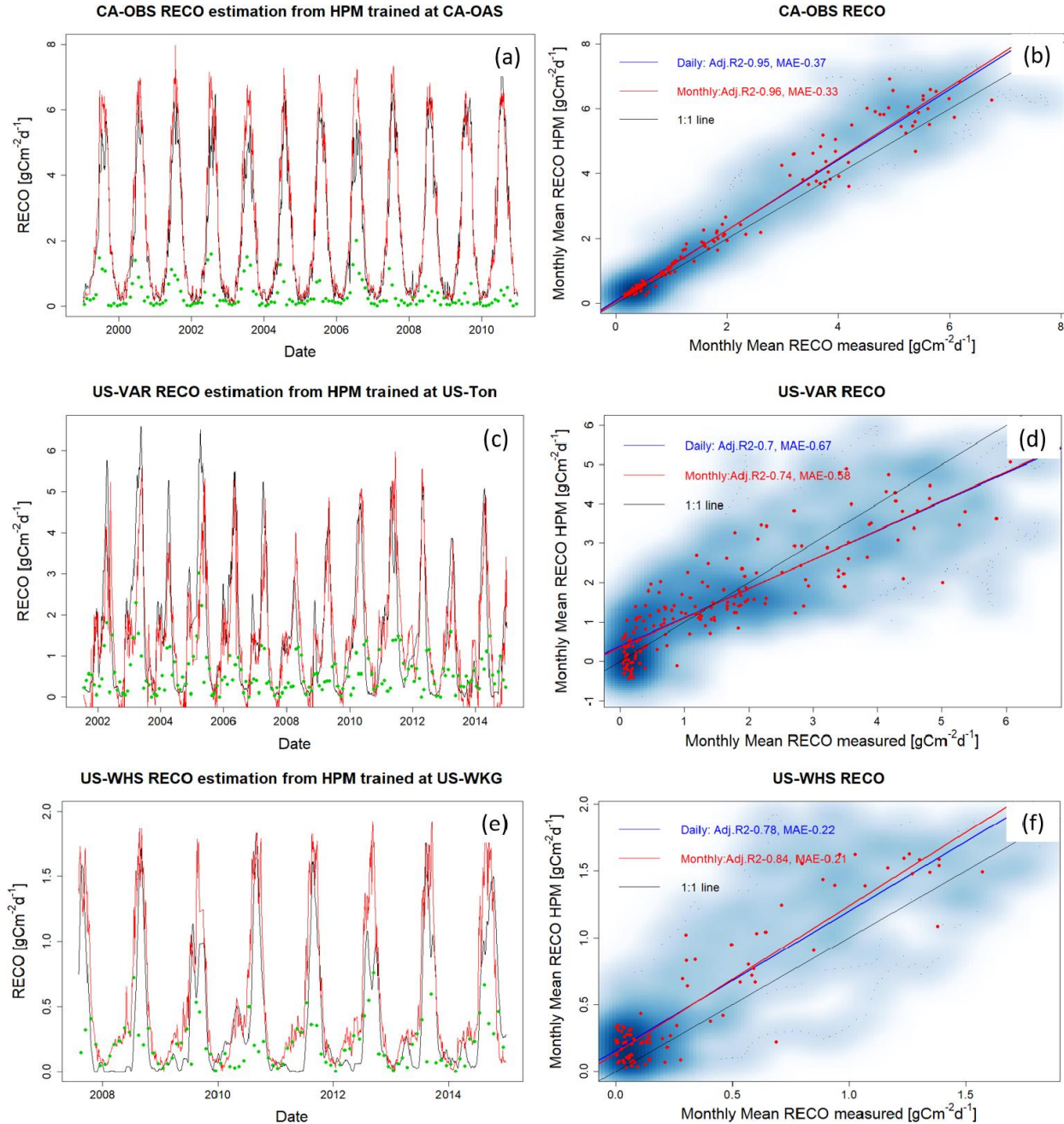


Figure 8. $RECO$ estimation at CA-Oas (a), US-Var (c), and US-Whs (e) with HPM trained at US-Ton, US-Wkg, and CA-Oas, respectively. Red and black lines represent HPM estimations and real measurements; green points denote the monthly mean difference between HPM estimation and measurements. Panels (b), (d), and (f) show the scatter plots of daily (blue) and monthly (red) $RECO$ at these three sites. Darker blue clouds represent greater density of data points.

4.3 Use Case 3: Ecoregion-Based, Mechanistic HPM Estimation of ET

Mechanistic HPM, which is trained with ET estimates from 1-D physically-based-model simulations, provides an avenue for estimating ET in ecoregions where direct measurements from eddy covariance tower are not

available. In order to test the effectiveness of the mechanistic HPM, we focused on the three SNOTEL stations and US-NR1, which locates in the “Western Cordillera” ecoregion. Mechanistic HPM is coupled with CLM simulations at these sites (Tran et al., 2019). To ensure the CLM physically-based-model simulations can provide alternative datasets to develop mechanistic HPMs, we compared CLM estimation and direct measurements of ET at US-NR1 (Figure S2). The consistent results between measured ET and CLM-estimated ET (adjusted $R^2 = 0.88$; $k = 0.95$) indicate independent CLM simulations can be effectively used to develop the mechanistic HPM.

We applied mechanistic HPM trained with 1-D CLM developed at ER-BT (Tran et al., 2019) to estimate ET at sites classified as part of the same ecoregion (i.e., ER-SP, ER-PK and US-NR1). We then compared ET estimation from HPM to independent CLM-based ET estimations at ER-SP and ER-PK and to direct measurements at US-NR1. Figure 9 shows a high consistency between HPM estimation and the validation data. For all scenarios, an adjusted R^2 of 0.8 or greater is observed (Table 54), which strongly indicates that mechanistic HPM can provide accurate ET estimation at sites of similar ecoregions. These results suggest the broad applicability of mechanistic HPM to estimate ET based on ecoregion characteristics. This approach is expected to be particularly useful for regions where flux towers are difficult to install or where measured fluxes are not representative of the landscape, such as in mountainous watersheds.

Table 54. Statistical summary of HPM estimation over space with FLUXNET sites and SNOTEL stations with CLM

Target Site	Training Site	Level II Ecoregion	ET MSE (monthly)[mm/d]	ET Adj. R^2	R_{ECO} MSE(monthly)[$gCm^{-2}d^{-1}$]	R_{ECO} Adj. R^2
CA-Obs	CA-Oas	Boreal Plain	0.39	0.88	0.36	0.97
US-Var	US-Ton	Mediterranean California	0.34	0.70	0.67	0.70
US-Whs	US-Wkg	Western Serra Madre Piedmont	0.13	0.94	0.17	0.85
ER-SP	ER-BT	Western Cordillera	0.20	0.92	-	-
ER-PK	ER-BT	Western Cordillera	0.24	0.90	-	-
US-NR1	ER-BT	Western Cordillera	0.23	0.90		

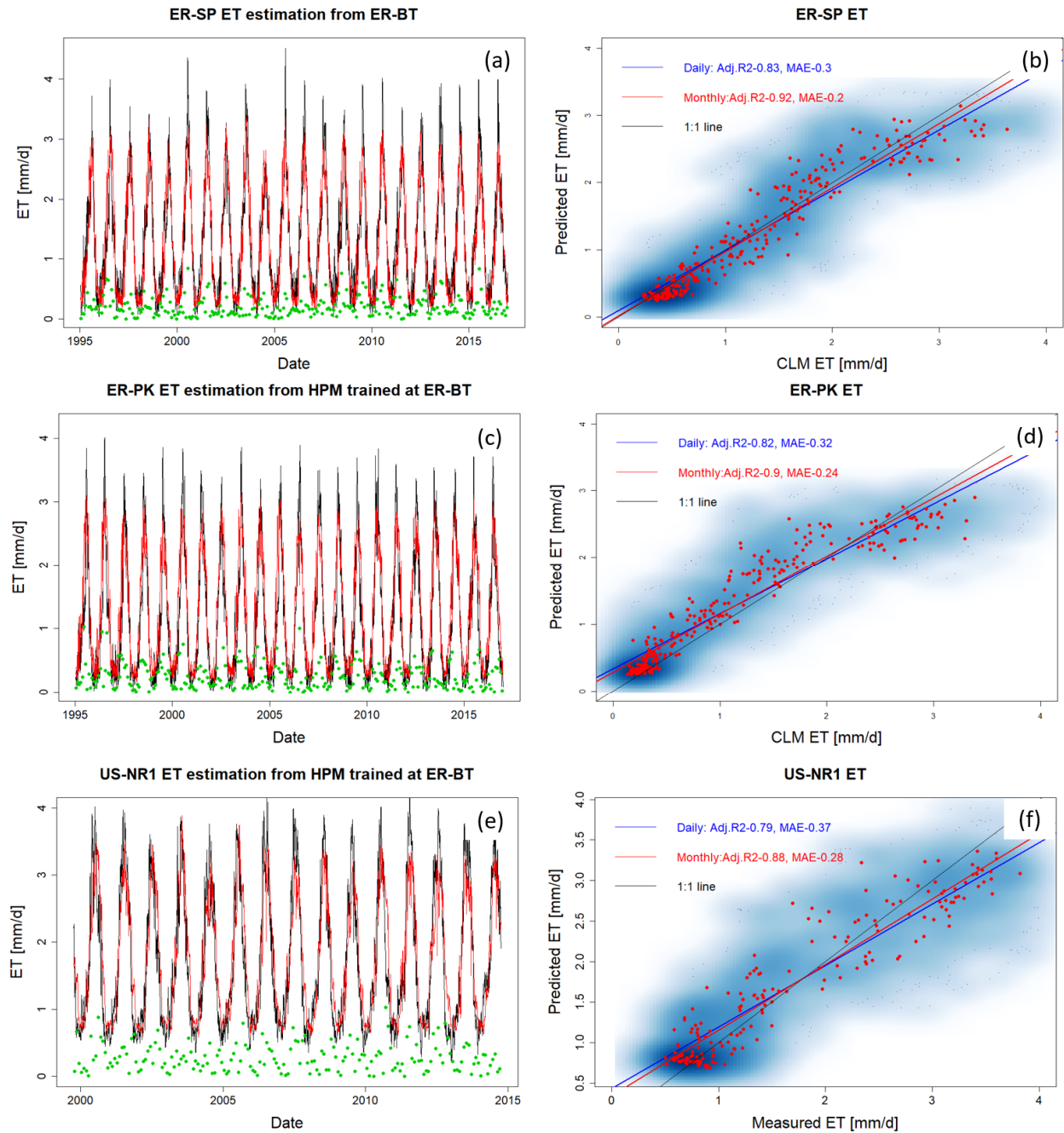


Figure 9. HPMs trained with CLM simulation at ER-BT are used to estimate ET at ER-SP, ER-PK, and US-NR1. Panels (a), (c), and (e) display HPM estimation of ET (red lines), as well as independent CLM estimation at ER-SP, ER-PK, and eddy covariance measurements at US-NR1 (black lines). Panels (b), (d), and (f) show the scatter plots of daily (blue) and monthly (red) ET at these three sites. Darker blue clouds represent greater density of data points.

4.4 Exploration of How ET and R_{ECO} Varies with Meteorological forcings and Vegetation Heterogeneity at the East River Watershed

ET and R_{ECO} estimated from the HPM model at the mountainous East River Watershed in CO enabled us to analyze how vegetation heterogeneity and meteorological forcings heterogeneity influence estimated ET and R_{ECO}

dynamics, and to identify limitations in the developed approach for estimating ET and R_{ECO} across mountainous and heterogeneous watersheds.

NDVI time-series data provide high-resolution (30m scale) information about vegetation variability across the East River Watershed. The spatial distribution of vegetation cover presented in Figure 2 (from Falco et al. 2019) enables us to distinguish different patches of deciduous forests, evergreen forests, meadow grassland and riparian shrublands and retrieve corresponding NDVI time-series. NDVI time series is related with snowmelt processes, whereas earlier snowmelt triggers earlier vegetation growth and result in earlier rise NDVI values (Pedersen et al., 2018). Figure 10 shows Landsat-derived and reconstructed NDVI values for the four different vegetation types within the East River Watershed. Evergreen forests have an extended growing season compared to deciduous forests. However, peak NDVI is smaller in evergreen forests compared to deciduous forests. March, April and May mean NDVI values in 2012 for site DF1 are 0.07, 0.22 and 0.37 respectively compared to 0.06, 0.15 and 0.33 in 2015. The early rise of NDVI values observed in April 2012 is consistent with the fact that snowmelt occurred much earlier in 2012 than in 2015, as recorded by the SNOTEL Butte station. Earlier increase of NDVI in earlier snowmelt year (2012) was also observed for other vegetation types. In addition, evergreen forests have an extended growing season compared to the other vegetation types. For example, March-mean NDVI for EF1, RS1 and MS1 in 2012 are 0.30, 0.13, 0.11 compared to 0.28, 0.11, 0.08 in 2015, respectively whereas May-mean NDVI for EF1, RS1 and MS1 in 2012 are 0.38, 0.33, 0.35 compared to 0.34, 0.29 and 0.31 in 2015, respectively. Though earlier snowmelt triggers earlier increase in vegetation growth, significant faster greenness was observed for deciduous forests, meadow grasslands and shrublands compared to evergreen forests, where NDVI increased by 0.08, 0.20, 0.24 and 0.30 for evergreen forests, shrublands, grasslands and deciduous forests in 2012, respectively. In addition, peak NDVI is generally smaller in evergreen forests compared to deciduous forests, meadow grasslands and riparian shrublands. NDVI ranges from 0.2 to 0.6 for evergreen forests, whereas larger fluctuations in NDVI are observed for deciduous forests (-0.2 to 0.8), shrublands and grasslands. The NDVI values during the winter are likely sensing both snow and forest density, due to pixel spatial averaging from Landsat images. Similar to Qiao et al. (2016), we also found that the NDVI of deciduous forests exhibits a significant increase during the growing season, followed by a sharp decline (likely caused by defoliation), and that evergreen forests had a more stable NDVI. Similar sharp decreases in the NDVI of riparian shrublands and meadow grasslands are observed.

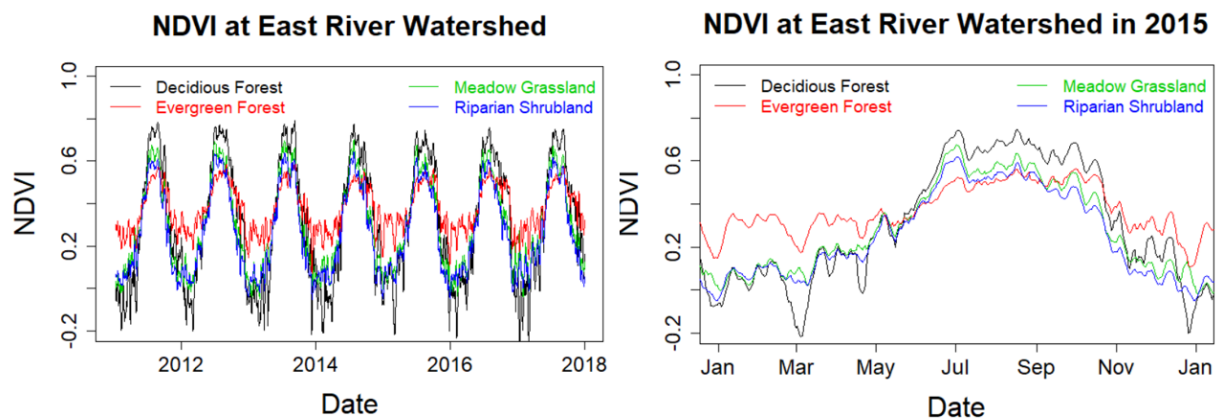


Figure 10: Reconstructed NDVI time series at selected locations in the East River Watershed for 2011 to 2018 (panel a) and for 2015 (panel b, normal water year). Black, red, green, and blue lines represent the time series of NDVI for deciduous forests, meadow grasslands, evergreen forests and riparian shrubland, respectively.

HPM-estimated ET and R_{ECO} also show different dynamics ~~in evergreen forests and deciduous forests with different vegetation types as a result of differences in snowmelt timing, meteorological forcing and vegetation heterogeneity.~~ Figure 11a and 11b present the time series of estimated ET and R_{ECO} associated with deciduous forests, respectively. Figure 11c and d present the ET and R_{ECO} differences between deciduous forests sites and ~~sites with other vegetation (e.g., evergreen forests shown in red), shrublands and grasslands.~~ Before peak growing season, ~~evergreen forests have the greatest ET and R_{ECO} compared to the other vegetation types.~~ ET of evergreen forests is about 10% greater than deciduous forests, whereas ET of deciduous forests during peak growing season is greater than evergreen forests, ~~shrublands and meadows.~~ After growing season, the NDVI of deciduous forests is less than 0.2 (loss of leaves) compared to the NDVI of evergreen forests. Before peak growing season, R_{ECO} of evergreen forests is slightly greater than deciduous forests, ~~meadow grasslands and shrublands.~~ During peak growing season, ~~we observed largest R_{ECO} for deciduous forests sites ($\sim 6 \text{ gCm}^{-2}\text{d}^{-1}$) followed by meadows, shrublands and evergreen forests.~~ R_{ECO} of deciduous forests is around 17% greater than R_{ECO} of evergreen forests. ~~Total-However, we did not observe significant differences in annual ET between evergreen and deciduous forests is very close (among these four vegetation types (e.g., DF1: 535 to 573 mm, MS1: 534 to 570 mm, RS1: 532 to 567 mm and EF1: 532 to 569 mm across 7 years in this study). Total annual R_{ECO} of evergreendeciduous forests is smallergreater than deciduous forests the other vegetation types (DF1: 642 to 698 $\text{gCm}^{-2}\text{d}^{-1}$, MS1: 588 to 636 gCm^{-2} , RS1: 589 to 636 gCm^{-2} and EF1: 592 to 639 gCm^{-2}).~~

Considering the inter-annual variability in snow dynamics, we observed annual ET at 569 mm and 532 mm and annual R_{ECO} at 639 gCm^{-2} and 602 gCm^{-2} at EF1 for 2012 and 2015, respectively. We observed an earlier increase in ET and R_{ECO} in 2012 with March-mean ET and R_{ECO} at 0.69 mm/day and 0.51 $\text{gCm}^{-2}\text{d}^{-1}$ compared to 0.60 mm/day and 0.47 $\text{gCm}^{-2}\text{d}^{-1}$ in 2015. During peak growing season, we observed July-mean ET at 3.43 and 3.33 mm/day and R_{ECO} at 4.73 and 4.47 0.47 $\text{gCm}^{-2}\text{d}^{-1}$ for 2012 and 2015, respectively. Though earlier snowmelt usually triggers summer drought conditions, we observed a significantly greater amount of monsoon precipitation in 2012 (3.06 mmd^{-1}) compared to 2015 (1.87 mmd^{-1}). Water stress situation caused by earlier snowmelt was largely compensated by earlier monsoon in 2012, and thus we observed higher March, July and annual ET and R_{ECO} compared to 2015. Similar trends have also been observed for deciduous forests, shrublands and meadows in 2012 and 2015.

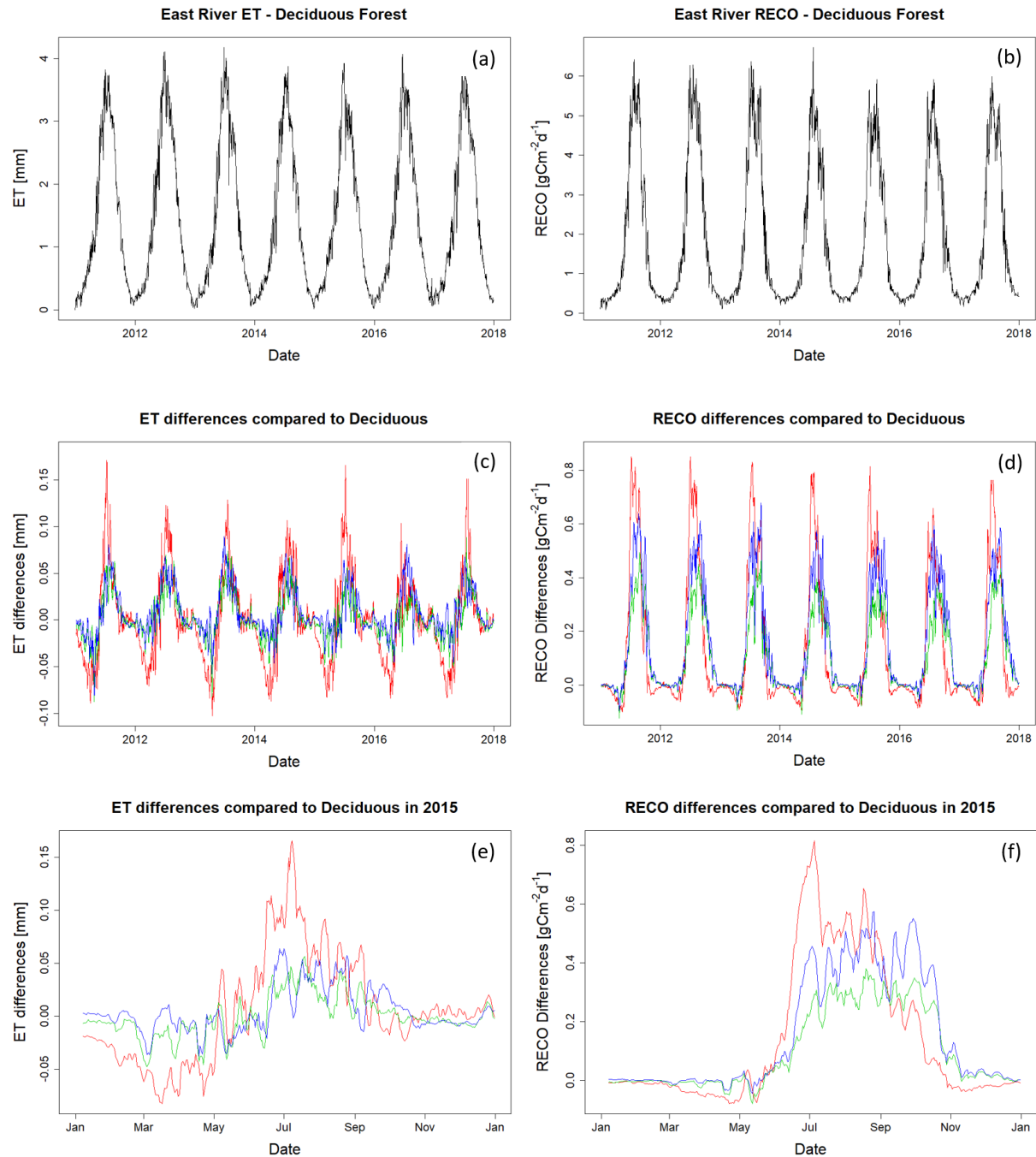


Figure 11: ET (a) and R_{ECO} (b) estimation for the deciduous forest site DF1 at the East River Watershed. Panels (c) and (d) show the differences in ET and R_{ECO} among various vegetation types and DF1. Red, green, and blue lines represent the differences in evergreen forest, meadow, and riparian shrubland compared to DF1. Panels (e) and (f) zoom into 2015 to better display seasonal variations.

ET and R_{ECO} estimation at the East River Watershed from the HPM model further enabled us to assess the role of input attributes and investigate limitations of the HPM approach. Figure 12 shows the absolute value of monthly

mean difference in ET (Fig. 12a and Fig. 12b) and R_{ECO} (Fig. 12c and Fig. 12d) across SNOTEL stations (ER-BT, ER-SP and ER-PK) and within selected East River locations. Landsat data enabled us to capture NDVI differences at these sites (Figure 10), but we have identified the insufficient resolution of input meteorological forcing data at the East River sites. We observed a greater differences in temperature and radiation at the SNOTEL sites whereas there's very small differences at the East River sites (Figure S3). Summer temperature differences among SNOTEL sites can be over 3 °C but there's a barely 0.2 °C differences in DAYMET data used for the East River sites. In addition, a ~80 W/m^2 of radiation differences is observed with SNOTEL data whereas radiation differences stays around 30 W/m^2 for East River sites. Correspondingly, we observed 2.5 times greater differences in ET across SNOTEL stations compared to the sites within the East River watershed. We observed similar level of differences (around 0.8 gCm^{-2}) in R_{ECO} within East River Watershed and across SNOTEL stations. These results indicate HPM ET model is sensitive to temperature and radiation inputs whereas NDVI, temperature and radiation are all influential for HPM R_{ECO} models. Differences in ET and R_{ECO} among SNOTEL sites and East River sites are resulted from the differences in input meteorological forcing data. If high resolution meteorological data becomes available for the East River watershed, we believe the HPM approach can better capture heterogeneities in ET and R_{ECO} at the East River watershed and better distinguish the roles of meteorological forcing and vegetation heterogeneity on ET and R_{ECO} distribution.

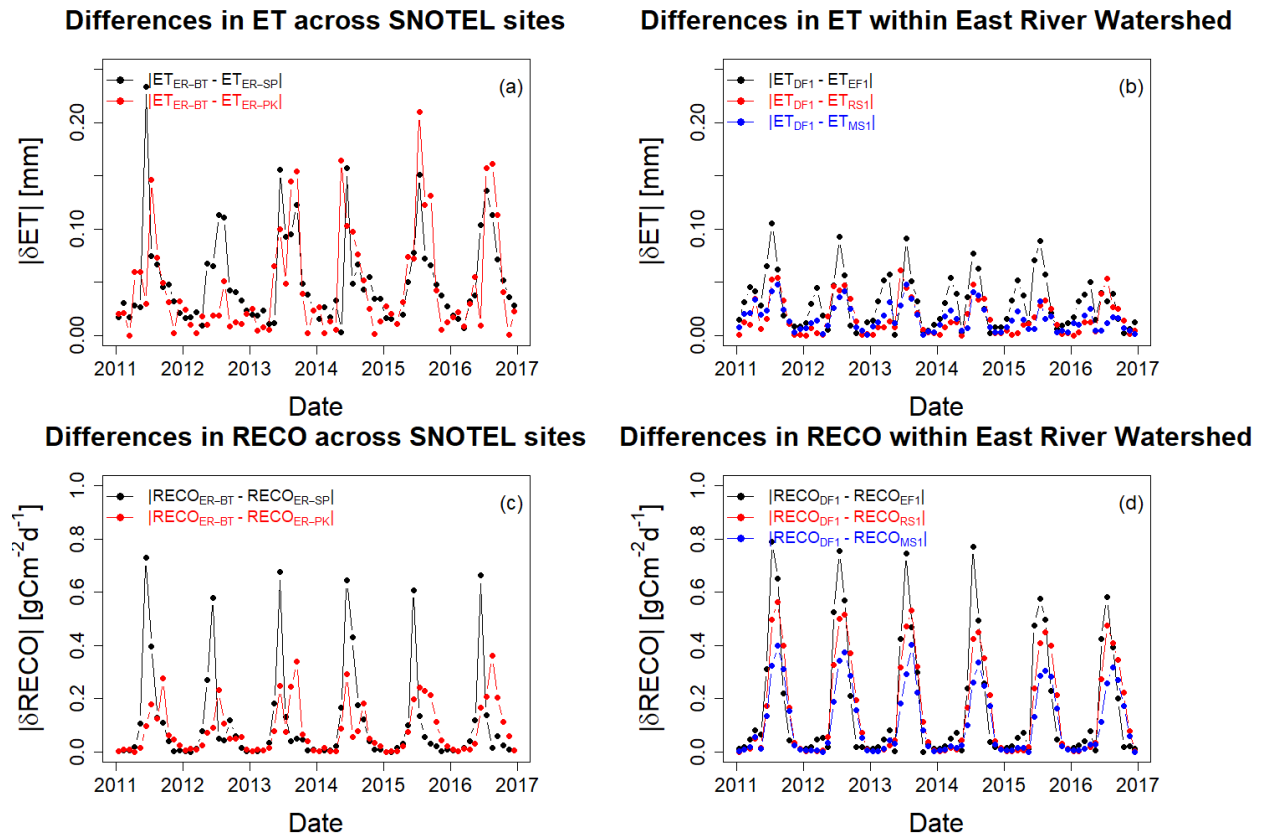


Figure 12. Absolute differences in monthly mean ET and R_{ECO} across SNOTEL stations and within East River Watershed. Panels (a) and (c) describe the absolute differences in monthly mean ET and R_{ECO} between ER-BT, ER-SP, and ER-PK.

Panels (b) and (d) describe the absolute differences in monthly mean ET and R_{ECO} within East River Watershed between deciduous forest (DF1), evergreen forest (EF1), meadow (MS1), and riparian shrubland (RS1).

5. Discussion

Our study demonstrates that HPM provides reliable estimations of ET and R_{ECO} under various climate and vegetation conditions, including data-based HPMs that are trained with FLUXNET data as well as physical-model-based HPMs that are coupled with simulations results from mechanistic models (i.e., CLM in this study). With 70% of the data used for training (model development), ET and R_{ECO} estimation from HPM achieves an adjusted R^2 of 0.9 compared to eddy covariance measurements. With this high estimation accuracy, we demonstrated that this approach could be used for predicting ET and R_{ECO} over time. HPM is capable of “learning” the complex interactions among meteorological forcings, vegetation dynamics, and water and carbon fluxes. The underlying relationships acquired by HPM can serve as a local ecohydrological model for long-term monitoring of ET and R_{ECO} with the aid of remote sensing data, and can fill in gap data during occasional equipment failure. HPM was also successful at estimating the spatial distribution of ET and R_{ECO} through exploiting an ecoregion concept. Using the representative FLUXNET sites in different ecoregions, HPM provided estimates of ET and R_{ECO} at locations using learned relationships from other sites having the same ecoregion classification. For conditions where no FLUXNET sites are within the same ecoregion, our study showed that physically-based models that utilize weather forcings data can provide alternatives for developing mechanistic HPM to estimate ET and R_{ECO} .

With the proposed HPM approach, we investigated the variability in ET and R_{ECO} estimations across different proportions of the East River Watersheds. While we currently do not have continuous measurements of ET and R_{ECO} at the East River Watershed for validation, our results are comparable to other studies that focus on sites within the same ecoregion. HPM-based ET estimation at East River Watershed is comparable to Mu et al. (2013), where ET is computed based upon the logic of the Penman-Monteith equation and MODIS remote sensing data. At the East River Watershed, data retrieved from Mu et al. (2013) indicate annual ET ranges from 554 to 585 mm at deciduous forests sites and 540 to 593 mm at evergreen forests sites. The R^2 between 8 day aggregated HPM based ET estimation and data retrieved from Mu et al. (2013) achieves 0.65 (Figure S1). Berryman et al. (2018) developed a random forest model to predict growing season soil respiration at subalpine forests in the Southern Rocky Mountain ecoregions. Their results suggest a consistent respiration rate from 2004 to 2006, with 150 day sums of 542.8, 544.3 and 536.5 gCm^{-2} , respectively, with a mean measured growing season respiration across sites and years of 3.37 gCm^{-2} . HPM based R_{ECO} estimation is also (Figure S1), and the HPM-based R_{ECO} estimation is comparable to what Berryman et al. (2018) discovered, with growing season R_{ECO} ranging between 555 to 607 gCm^{-2} and mean growing season R_{ECO} ranging between 3.01 to 3.30 gCm^{-2} . While we currently do not have a time series measurement of ET and R_{ECO} at the East River Watershed for validation, our results are comparable to other studies that focus on sites within the same ecoregion (e.g., Annual ET between deciduous forests and evergreen forests are not statistically different, which is similar to Mu et al. (2013). Annual R_{ECO} differences between evergreen forests and deciduous forests are around 50 gCm^{-2} , which is comparable to Berryman et al., 2018).

We confirmed the important role of

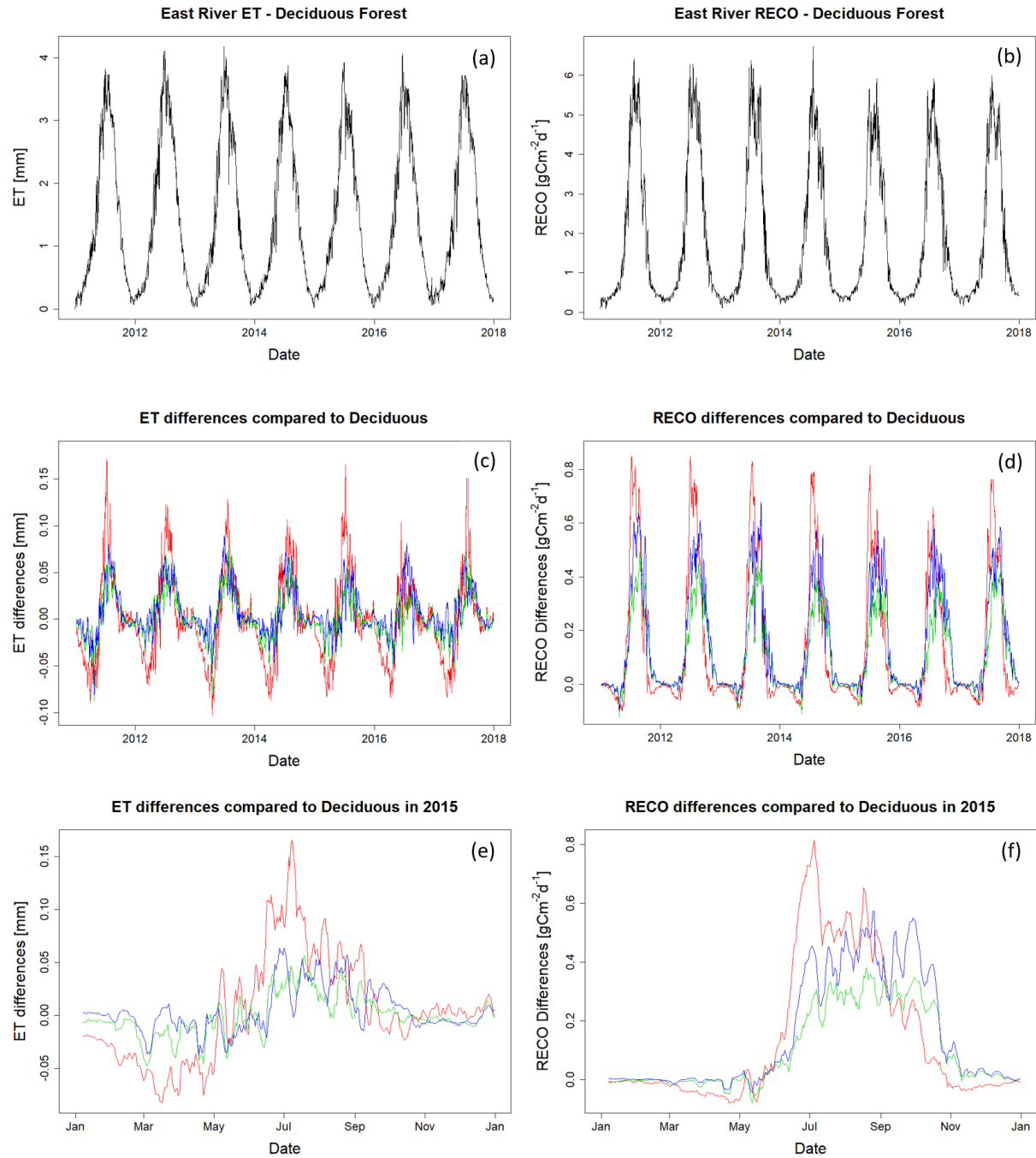


Figure 11: ET (a) and R_{ECO} (b) estimation for the deciduous forest site DF1 at the East River Watershed. Panels (c) and (d) show the differences in ET and R_{ECO} among various vegetation types and DF1. Red, green, and blue lines represent the differences in evergreen forest, meadow, and riparian shrubland compared to DF1. Panels (e) and (f) zoom into 2015 to better display seasonal variations.

ET and R_{ECO} estimation at the East River Watershed from the HPM model further enabled us to assess the impacts of small scale (e.g., hillslope scale) heterogeneity in vegetation type on ET and R_{ECO} dynamics. Figure 12 shows the absolute value of monthly mean difference in ET (Fig. 12a and Fig. 12b) and R_{ECO} (Fig. 12c and Fig. 12d) across SNOTEL stations (ER-BT, ER-SP and ER-PK) and within selected East River locations. A comparison of meteorological forcings data within selected East River locations and across SNOTEL stations are given in Figure S3. We observed 2.5 times greater differences in ET across SNOTEL stations compared to the sites within the East River watershed, whereas the differences in R_{ECO} across SNOTEL stations are at the same level compared to the sites within East River Watershed (around 0.8 gCm^{-2}). This result indicates small scale meteorological forcings and vegetation heterogeneity are the major controls of differences in ET and R_{ECO} at the East River Watershed.

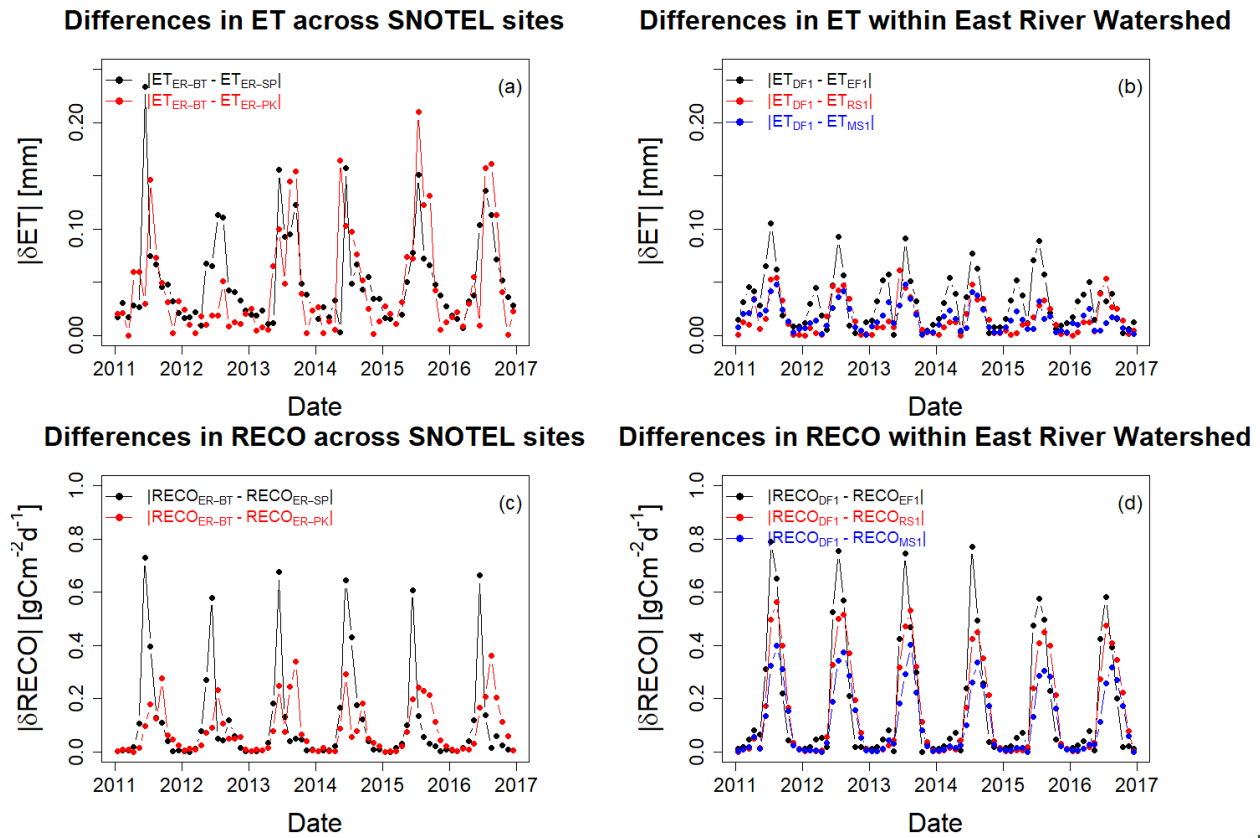


Figure 12. Absolute differences in monthly mean ET and R_{ECO} across SNOTEL stations and within East River Watershed. Panels (a) and (c) describe the absolute differences in monthly mean ET and R_{ECO} between ER-BT, ER-SP, and ER-PK. Panels (b) and (d) describe the absolute differences in monthly mean ET and R_{ECO} within East River Watershed between deciduous forest (DF1), evergreen forest (EF1), meadow (MS1), and riparian shrubland (RS1).

5. Discussion

Our study demonstrates that HPM provides reliable estimations of ET and R_{ECO} under various climate and vegetation conditions, including data-based HPMs that are trained with FLUXNET data and physical model-based HPMs that are coupled with simulations results from mechanistic models (i.e., CLM in our case). With 70% of the

data used for training (model development), ET and R_{ECO} estimation from HPM achieves an adjusted R^2 of 0.9 compared to eddy covariance measurements. With this high estimation accuracy, we demonstrated that this approach could be used for predicting ET and R_{ECO} over time. HPM is capable of “learning” the complex interactions among meteorological forcings, vegetation dynamics, and water and carbon fluxes. The underlying relationships acquired by HPM can serve as a local ecohydrological model for long term monitoring of ET and R_{ECO} , with the aid of remote sensing data, and can fill in gap data during occasional equipment failure.

HPM was also successful at estimating the spatial distribution of ET and R_{ECO} through exploiting an ecoregion concept. Using the representative FLUXNET sites in different ecoregions, HPM provided estimates of ET and R_{ECO} at locations using learned relationships from other sites having the same ecoregion classification. For conditions where no FLUXNET sites are within the same ecoregion, our study showed that physically based models that can utilize weather forcings data can provide alternatives for developing mechanistic HPM to estimate ET and R_{ECO} . We found that HPM performance was more reliable when trained and applied at different watersheds in the same ecoregion. For example, HPM that only relies on energy related parameters was able to successfully estimate ET and R_{ECO} at US NR1 and CA OAS, where radiation and temperature are key components that regulate ET and R_{ECO} dynamics. However, HPM with the same input features do not yield desired results at sites limited by water conditions (e.g., US Ton and US Var), due to lack of soil moisture data. This change indicates that parameter optimization and attributes selection may be needed for sites that are limited by moisture conditions, because important features can be subject to local conditions that potentially lower HPM performance.

We confirmed the important role of small-scale vegetation heterogeneity in modeling ET and R_{ECO} dynamics, which further enabled us to better understand ecosystem dynamics at the East River Watershed. As indicated from NDVI time series (Fig 10), evergreen forests have a longer growing season compared to deciduous forests/other vegetation types; however, deciduous forests have greater/higher peak NDVI values. Correspondingly, we also observed an earlier increase in ET and R_{ECO} for evergreen forests (before May), but larger ET and R_{ECO} for deciduous forests during peak growing season (around June and July). Annual ET between deciduous forests and evergreen forests are not statistically different, which is similar to (Berryman et al., 2018; Mu et al., 2013). Similar dynamics were also observed at regions that have different climate conditions. Annual R_{ECO} differences between evergreen forests and deciduous forests are around 50 gCm^{-2} , which is comparable to (Berryman et al. 2018). Similar dynamics were also observed at regions that have different climate conditions. Through assessing the differential mechanisms of deciduous forests and evergreen forests at various sites under Mediterranean climates, Baldocchi et al. (2010) found that deciduous forests had a shorter growing season, but showed a greater capacity for assimilating carbon during the growing season. Evergreen forests, on the other hand, had an extended growing season but with a smaller capacity for gaining carbon. These results were identified through analyzing the relationships among leaf ages, leaf nitrogen level, leaf area, and water use efficiencies of these tree species at the selected Mediterranean sites. Older/They found older leaves tend to have smaller leaf nitrogen and stomata conductance, and thus that lead to smaller ET and R_{ECO} during peak growing seasons. Though our approach were not able to quantify the physiology differences among vegetation types, HPM estimation indicated evergreen forest/forests that maintain leaves throughout the year have smaller ET and

R_{ECO} are smaller during the peak growing season compared to deciduous forests, yet maintain a relatively high level before the peak other vegetation types.

Dynamic changes in the inter-annual variability of meteorological conditions result in varying growing season or during defoliation length and spatiotemporal variability in ET and R_{ECO} . Earlier snowmelt triggers earlier growth of vegetation, causing earlier rise in ET and R_{ECO} . However, earlier growth in vegetation and increasing demand for water results in drought conditions (Sloat et al., 2015; Wainwright et al., 2020) that decrease ET and R_{ECO} . Timing and amount of monsoon precipitation are also important monsoons can relieve water stress and lead to increases in ET and R_{ECO} . Combination of these events jointly determine the magnitude of annual ET and R_{ECO} . Hu et al. (2010) analyzed flux data at US-NR1 to determine the relationships between growing season lengths and carbon sequestration, and found that extended growing season length resulted in less annual CO_2 uptake. They also found that the duration of growing seasons substantially decreases snow water storage, which significantly decreases forest carbon uptake. While we were not able in this study to assess the differential advantages and physiological mechanisms among vegetation types, HPM based estimation of ET and R_{ECO} presented similar dynamic trends to those found in Berryman et al. (2018); Hu et al. (2018); and Mu et al. (2013). Wieder et al. (2017) used point-scale CLM to better understand how complex terrain controls landscape-level variation of water, carbon and energy fluxes in the Niwot Ridge mountain ecosystems. With synthetic scenarios (e.g., different snow accumulation dynamics, fluctuations in air temperature), their simulation indicated earlier snowmelt and warmer summertime temperatures might drive divergent plant responses across the landscape. In our study, the combination of early snowmelt and early vegetation growth resulted in higher March ET and R_{ECO} in 2012 compared to 2015. The earlier start of growing season led to occurrences of fore-summer drought that decreases ET and R_{ECO} . However, the substantial earlier monsoon precipitation in 2012 relieved subsurface water stress whereas we observed higher July ET and R_{ECO} compared to other years. In addition, we observed smaller annual ET and R_{ECO} for evergreen forests that have longer growing season compared to other vegetation types. These results suggested HPM is capable of translating these variabilities in meteorological forcing and vegetation variables to ET and R_{ECO} dynamics.

Microclimate and small-scale heterogeneity in meteorological forcings attributes control the magnitude and timing of ET and R_{ECO} dynamics. For example, other Through comparing the HPM estimation results at different ecoregions, we also identified and assessed the limitations of current selection of input parameters. In the current study, we only used meteorological forcing and remote sensing based variables as inputs for HPM models, because these data are generally acquirable from weather reanalysis datasets and remote sensing products. HPM models with these variables provided reasonable estimates of ET and R_{ECO} for ecoregions limited by energy conditions, however we observed a decreasing prediction accuracy for ecoregions that experience seasonally dry periods. For example, HPM estimates at US-NR1 and CA-OAS achieved very high R^2 and small MAE; but prediction accuracy decreases especially during peak growing season at US-Ton and other water-limiting sites. These results indicate other key variables are necessary in order to capture dynamics during the seasonally dry periods, such as soil moisture measurement. The current HPM models did not use soil moisture as an input variable due to data availability reasons,

but we believe and recommend adding soil moisture as well as other key variables to HPMs to further improve model performance at these seasonally dry ecoregions when such data becomes available.

Parameterization and spatiotemporal resolution of meteorological forcing data still remain a challenge for improving ET and R_{ECO} estimation at sparsely monitored watersheds. Microclimate and heterogeneities in meteorological forcing attributes control the magnitude and timing of ET and R_{ECO} dynamics. Other field observations along the Rocky Mountain ranges have shown that south-facing hillslopes have significantly earlier snowmelt compared to north-facing hillslopes (Kampf et al., 2015; Webb et al., 2018), which are hypothesized to result in significant differences in ET and R_{ECO} dynamics. ~~As a result, estimation of small-scale~~ We compared ET and R_{ECO} dynamics requires high spatial resolution meteorological inputs, which is currently a challenge. We originally intended to investigate aspect impacts on ET differences among SNOTEL sites and R_{ECO} dynamics at East River Watershed by selecting sites and identified ET differences among SNOTEL sites are greater than the differences among East River sites with different slope orientations. However, small-scale meteorological forcings but R_{ECO} differences are similar between the two groups. Data from weather stations (SNOTEL sites) captured the spatiotemporal heterogeneity and microclimate were not available due to the relatively low spatial resolution of meteorological forcings inputs (DAYMET, 1 km scale). While in radiation and temperature, however DAYMET data suggest that differences in air temperature and solar radiation are suggested very small for sites located at different portions of the watershed, the three weather stations at the site reveal that spatial heterogeneity differences in radiation and temperature (Figure S3 and S4). The insufficient spatial resolution of input meteorological forcing attributes do exist, especially air temperature (Figure S4). Even though the small-scale meteorological forcings heterogeneity is partly embedded in NDVI time series, the heterogeneity in ET and R_{ECO} estimated from data limits HPM performance at the East River Watershed is potentially underestimated, due to the insufficient spatial resolution of meteorological inputs. In addition to limitations imposed from the spatial resolution, uncertainties. Uncertainties in meteorological inputs can also result in large errors (i.e., >20% MAE) and reduce accuracy by 10-30% in ET and R_{ECO} estimations as suggested by Mu et al. (2013) and Zhang et al. (2019). Thus, there is still a significant need for high-spatial-resolution meteorological-forcing data products, such as data provided by the Surface Atmosphere Integrated Field Laboratory (SAIFL) that can capture small-scale heterogeneity for implementing into HPM, which will then to enable us to better estimates of ET and R_{ECO} , and assess the governing factors that regulate small-scale heterogeneity in ET and R_{ECO} their spatiotemporal variability.

In addition to the quality of meteorological data, HPM is also influenced by remote sensing inputs accuracy. Incorrectly calculated or pixel-averaged NDVI values from Landsat images can greatly alter HPM outputs for ET and R_{ECO} . Satellite images with different cloud cover have a slight influence over the NDVI values calculated, which do not represent real-time vegetation conditions. Algorithms used to reconstruct daily NDVI time series are also subject to uncertainties. However, But with recent advances in remote sensing and satellite technologies (McCabe et al., 2017), the spatial and temporal resolution should greatly increase in the future (i.e., and harmonized Landsat-Sentinel datasets (Claverie et al., 2018), the spatial and temporal resolution should greatly increase in the future (i.e., 3 m resolution

and daily). These advances will lead to more accurate classification of vegetation types and NDVI calculations, which are expected to decrease uncertainty associated with flux estimation

Another source of uncertainty in HPM arises from the choice of hybrid approaches and any parameter uncertainties in mechanistic models. Since HPM relies on accurate ET and R_{ECO} inputs from flux towers or mechanistic models, any uncertainties in measuring or modeling ET and R_{ECO} will propagate to HPM. If HPM is developed with a mechanistic model that has such missing components, these biases will be passed on to HPM estimation of ET and R_{ECO} . Parameter and conceptual model uncertainties in mechanistic models also restrict HPM's ability to "learn" the ecosystem dynamics. In order to reduce potential biasedness, we trained data-based HPM and physical-model-based HPM upon long time series (e.g., > 5 years) with quality assessed data or simulation results, which also enables HPM to better memorize long time dependencies of ecosystem dynamics. Though the quantification of uncertainties remains challenging, efforts have been made to lower these uncertainties using the technical advances described here.

6. Conclusion

In this study, we developed and tested a Hybrid Predictive Modeling (HPM) approach for ET and R_{ECO} estimation, with a focus on mountainous watersheds-in the Rocky Mountains. We developed individual HPM models at various FLUXNET sites and at sites where data can supports the proper development of a mechanistic model (e.g., CLM). These models were validated against eddy covariance measurements and CLM outputs. We further used these models for ET and R_{ECO} estimation at watersheds within the same ecoregion to test HPM's capability of providing estimation over space, where only meteorological forcings data and remote sensing data were available. Lastly, we applied the HPM to provide long-term estimation of ET and R_{ECO} and test the sensitivity of HPM to various vegetation types at various sites within the East River Watershed of CO.

Given the promising results of HPM, this work offers an avenue for estimating ET and R_{ECO} using easy-to-acquire or commonly available datasets. This study also suggests that the spatial heterogeneity of meteorological forcings and vegetation dynamics have significant impacts on ET and R_{ECO} dynamics, which may be currently underestimated due to typically coarse spatial resolution of data inputs. Parameters related to energy and soil moisture conditions can be implemented into HPM to increase HPM's accuracy, especially for sites in ecoregions limited by soil moisture conditions. Lastly, it should be pointed out that HPM is not restricted to estimation of ET and R_{ECO} only. We focused here on developing HPM for ET and R_{ECO} , but HPM also has great potential for estimating other parameters important for water and carbon cycles- given the right choice of input variables. Indeed, other attributes, such as GPPnet ecosystem exchange (Figure A6) and sensible heat flux, might also be accurately captured and represented with HPM, given the right choice of features.

Data availability. The data used in this study are from publicly available datasets. FLUXNET measurements can be accessed at <https://FLUXNET.fluxdata.org>. SNOTEL data are available at <https://www.wcc.nrcs.usda.gov/snow/>. DAYMET data can be found at (Thornton et al., 2017) or via Google Earth Engine. Landsat data are available on

Google Earth Engine. All data and simulated results and model parameters associated with this article can be found at <https://data.ess-dive.lbl.gov/view/doi:10.15485/1633810>.

Acknowledgement. This material is based upon work supported as part of the Watershed Function Scientific Focus Area funded by the U.S. Department of Energy, Office of Science, Office of Biological and Environmental Research under Award Number DE-AC02-05CH11231. We thank Haruko Wainwright and Bhavna Arora for providing comments on East River estimations. We also greatly appreciate all the guidance provided by Professor Yoram Rubin and Professor Dennis Baldocchi at UC Berkeley to the first author. We also acknowledge the Jane Lewis Fellowship Committee of the UC Berkeley for providing fellowship support to the first author.

References

- Abatzoglou, J. T., Barbero, R., Wolf, J. W. and Holden, Z. A.: Tracking Interannual Streamflow Variability with Drought Indices in the U.S. Pacific Northwest, *J. Hydrometeorol.*, doi:10.1175/jhm-d-13-0167.1, 2014.
- Ai, J., Jia, G., Epstein, H. E., Wang, H., Zhang, A. and Hu, Y.: MODIS-Based Estimates of Global Terrestrial Ecosystem Respiration, *J. Geophys. Res. Biogeosciences*, 123(2), 326–352, doi:10.1002/2017JG004107, 2018.
- Allen, R. G., Pereira, L. S., Raes, D. and Smith, M.: Crop evapotranspiration: Guidelines for computing crop requirements., 1998.
- Anderson, M. C., Allen, R. G., Morse, A. and Kustas, W. P.: Use of Landsat thermal imagery in monitoring evapotranspiration and managing water resources, *Remote Sens. Environ.*, doi:10.1016/j.rse.2011.08.025, 2012.
- Baldocchi, D.: Measuring fluxes of trace gases and energy between ecosystems and the atmosphere - the state and future of the eddy covariance method, *Glob. Chang. Biol.*, doi:10.1111/gcb.12649, 2014.
- Baldocchi, D. D., Ma, S., Rambal, S., Misson, L., Ourcival, J. M., Limousin, J. M., Pereira, J. and Papale, D.: On the differential advantages of evergreenness and deciduousness in mediterranean oak woodlands: A flux perspective, *Ecol. Appl.*, 20(6), 1583–1597, doi:10.1890/08-2047.1, 2010.
- Berryman, E. M., Vanderhoof, M. K., Bradford, J. B., Hawbaker, T. J., Henne, P. D., Burns, S. P., Frank, J. M., Birdsey, R. A. and Ryan, M. G.: Estimating Soil Respiration in a Subalpine Landscape Using Point, Terrain, Climate, and Greenness Data, *J. Geophys. Res. Biogeosciences*, 123(10), 3231–3249, doi:10.1029/2018JG004613, 2018.
- Bodesheim, P., Jung, M., Gans, F., Mahecha, M. D. and Reichstein, M.: Upscaled diurnal cycles of land-Atmosphere fluxes: A new global half-hourly data product, *Earth Syst. Sci. Data*, 10(3), 1327–1365, doi:10.5194/essd-10-1327-2018, 2018.
- ~~Breshears, D. D., Cobb, N. S., Rich, P. M., Price, K. P., Allen, C. D., Balice, R. G., Romme, W. H., Kastens, J. H., Floyd, M. L., Belnap, J., Anderson, J. J., Myers, O. B. and Meyer, C. W.: Regional vegetation die-off in response to global change type drought, *Proc. Natl. Acad. Sci. U. S. A.*, doi:10.1073/pnas.0505734102, 2005.~~
- De Bruin, H. A. R.: A model for the Priestley-Taylor parameter alpha., *J. Clim. Appl. Meteorol.*, doi:10.1175/1520-0450(1983)0222.0.CO;2, 1983.
- Budyko, M. I.: The Heat Balance of the Earth's Surface, *Sov. Geogr.*, 2(4), 3–13, doi:10.1080/00385417.1961.10770761, 1961.
- ~~Chang, L. L., Dwivedi, R., Knowles, J. F., Fang, Y. H., Niu, G. Y., Pelletier, J. D., Rasmussen, C., Durcik, M., Barron-Gafford, G. A. and Meixner, T.: Why Do Large-Scale Land Surface Models Produce a Low Ratio of Transpiration to Evapotranspiration?, *J. Geophys. Res. Atmos.*, doi:10.1029/2018JD029159, 2018.~~
- ~~Claverie, M., Ju, J., Masek, J. G., Dungan, J. L., Vermote, E. F., Roger, J. C., Skakun, S. V. and Justice, C.: The Harmonized Landsat and Sentinel-2 surface reflectance data set, *Remote Sens. Environ.*,~~

[doi:10.1016/j.rse.2018.09.002](https://doi.org/10.1016/j.rse.2018.09.002), 2018.

Cox, P. M., Betts, R. A., Jones, C. D., Spall, S. A. and Totterdell, I. J.: Acceleration of global warming due to carbon-cycle feedbacks in a coupled climate model, *Nature*, doi:10.1038/35041539, 2000.

Daggers, T. D., Kromkamp, J. C., Herman, P. M. J. and van der Wal, D.: A model to assess microphytobenthic primary production in tidal systems using satellite remote sensing, *Remote Sens. Environ.*, 211(April), 129–145, doi:10.1016/j.rse.2018.03.037, 2018.

~~Ernakovich, J. G., Hopping, K. A., Berdanier, A. B., Simpson, R. T., Kachergis, E. J., Steltzer, H. and Wallenstein, M. D.: Predicted responses of arctic and alpine ecosystems to altered seasonality under climate change, *Glob. Chang. Biol.*, doi:10.1111/geb.12568, 2014.~~

Falco, N., Wainwright, H., Dafflon, B., Léger, E., Peterson, J., Steltzer, H., Wilmer, C., Rowland, J. C., Williams, K. H. and Hubbard, S. S.: Investigating Microtopographic and Soil Controls on a Mountainous Meadow Plant Community Using High-Resolution Remote Sensing and Surface Geophysical Data, *J. Geophys. Res. Biogeosciences*, doi:10.1029/2018JG004394, 2019.

Gao, X., Mei, X., Gu, F., Hao, W., Li, H. and Gong, D.: Ecosystem respiration and its components in a rainfed spring maize cropland in the Loess Plateau, China, *Sci. Rep.*, doi:10.1038/s41598-017-17866-1, 2017.

Gao, Y., Yu, G., Li, S., Yan, H., Zhu, X., Wang, Q., Shi, P., Zhao, L., Li, Y., Zhang, F., Wang, Y. and Zhang, J.: A remote sensing model to estimate ecosystem respiration in Northern China and the Tibetan Plateau, *Ecol. Modell.*, doi:10.1016/j.ecolmodel.2015.03.001, 2015.

van Gorsel, E., Delpierre, N., Leuning, R., Black, A., Munger, J. W., Wofsy, S., Aubinet, M., Feigenwinter, C., Beringer, J., Bonal, D., Chen, B., Chen, J., Clement, R., Davis, K. J., Desai, A. R., Dragoni, D., Etzold, S., Grünwald, T., Gu, L., Heinesch, B., Hutya, L. R., Jans, W. W. P., Kutsch, W., Law, B. E., Leclerc, M. Y., Mammarella, I., Montagnani, L., Noormets, A., Rebmann, C. and Wharton, S.: Estimating nocturnal ecosystem respiration from the vertical turbulent flux and change in storage of CO₂, *Agric. For. Meteorol.*, 149(11), 1919–1930, doi:10.1016/j.agrformet.2009.06.020, 2009.

Greve, P., Gudmundsson, L., Orłowsky, B. and Seneviratne, S. I.: Introducing a probabilistic Budyko framework, *Geophys. Res. Lett.*, 42(7), 2261–2269, doi:10.1002/2015GL063449, 2015.

Hargrove, W. W. and Hoffman, F. M.: Using multivariate clustering to characterize ecoregion borders, *Comput. Sci. Eng.*, 1(4), 18–25, doi:10.1109/5992.774837, 1999.

Hargrove, W. W., Hoffman, F. M. and Law, B. E.: New analysis reveals representativeness of the amerflux network, *Eos (Washington, DC)*, 84(48), doi:10.1029/2003EO480001, 2003.

Hochreiter, S. and Schmidhuber, J.: Long Short-Term Memory, *Neural Comput.*, doi:10.1162/neco.1997.9.8.1735, 1997.

Homer, C., Dewitz, J., Yang, L., Jin, S., Danielson, P., Xian, G., Coulston, J., Herold, N., Wickham, J. and Megown, K.: Completion of the 2011 national land cover database for the conterminous United States – Representing a decade of land cover change information, *Photogramm. Eng. Remote Sensing*, doi:10.1016/S0099-1112(15)30100-2, 2015.

Hu, J., Moore, D. J. P., Burns, S. P. and Monson, R.: Longer growing seasons lead to less carbon sequestration by a subalpine forest, *Glob. Chang. Biol.*, 16(2), 771–783, doi:10.1111/j.1365-2486.2009.01967.x, 2010.

~~Hu, Z., Wang, G., Sun, X., Zhu, M., Song, C., Huang, K. and Chen, X.: Spatial Temporal Patterns of Evapotranspiration Along an Elevation Gradient on Mount Gongga, Southwest China, *Water Resour. Res.*, doi:10.1029/2018WR022645, 2018.~~

Hubbard, S. S., Williams, K. H., Agarwal, D., Banfield, J., Beller, H., Bouskill, N., Brodie, E., Carroll, R., Dafflon, B., Dwivedi, D., Falco, N., Faybishenko, B., Maxwell, R., Nico, P., Steefel, C., Steltzer, H., Tokunaga, T., Tran, P. A., Wainwright, H. and Varadharajan, C.: The East River, Colorado, Watershed: A Mountainous Community Testbed for Improving Predictive Understanding of Multiscale Hydrological–Biogeochemical Dynamics, *Vadose*

885 Zo. J., 17(1), 0, doi:10.2136/vzj2018.03.0061, 2018.

886 ~~Immerzeel, W. W., Lutz, A. F., Andrade, M., Bahl, A., Biemans, H., Bolch, T., Hyde, S., Brumby, S., Davies, B. J.,~~
887 ~~Elmore, A. C., Emmer, A., Feng, M., Fernández, A., Haritashya, U., Kargel, J. S., Koppes, M., Kraaijenbrink, P. D.~~
888 ~~A., Kulkarni, A. V., Mayewski, P., Nepal, S., Pacheco, P., Painter, T. H., Pellicciotti, F., Rajaram, H., Rupper, S.,~~
889 ~~Sinisalo, A., Shrestha, A. B., Viviroli, D., Wada, Y., Xiao, C., Yao, T. and Baillie, J. E. M.: Importance and~~
890 ~~vulnerability of the world's water towers, Nat. (in Press., 577(May 2019), 1–43, doi:10.1038/s41586-019-1822-y,~~
891 ~~2019.~~

892 IPCC: IPCC 2019- Special report on climate change, desertification, land degradation, sustainable land
893 management, food security, and greenhouse gas fluxes in terrestrial ecosystem, Res. Handb. Clim. Chang. Agric.
894 Law, doi:10.4337/9781784710644, 2019.

895 Irons, J. R., Dwyer, J. L. and Barsi, J. A.: The next Landsat satellite: The Landsat Data Continuity Mission, Remote
896 Sens. Environ., doi:10.1016/j.rse.2011.08.026, 2012.

897 Jägermeyr, J., Gerten, D., Lucht, W., Hostert, P., Migliavacca, M. and Nemani, R.: A high-resolution approach to
898 estimating ecosystem respiration at continental scales using operational satellite data, Glob. Chang. Biol.,
899 doi:10.1111/gcb.12443, 2014.

900 Jung, M., Reichstein, M., Ciais, P., Seneviratne, S. I., Sheffield, J., Goulden, M. L., Bonan, G., Cescatti, A., Chen,
901 J., De Jeu, R., Dolman, A. J., Eugster, W., Gerten, D., Gianelle, D., Gobron, N., Heinke, J., Kimball, J., Law, B. E.,
902 Montagnani, L., Mu, Q., Mueller, B., Oleson, K., Papale, D., Richardson, A. D., Rouspard, O., Running, S.,
903 Tomelleri, E., Viovy, N., Weber, U., Williams, C., Wood, E., Zaehle, S. and Zhang, K.: Recent decline in the global
904 land evapotranspiration trend due to limited moisture supply, Nature, doi:10.1038/nature09396, 2010.

905 Jung, M., Reichstein, M., Schwalm, C. R., Huntingford, C., Sitch, S., Ahlström, A., Arneth, A., Camps-Valls, G.,
906 Ciais, P., Friedlingstein, P., Gans, F., Ichii, K., Jain, A. K., Kato, E., Papale, D., Poulter, B., Raduly, B., Rödenbeck,
907 C., Tramontana, G., Viovy, N., Wang, Y. P., Weber, U., Zaehle, S. and Zeng, N.: Compensatory water effects link
908 yearly global land CO₂ sink changes to temperature, Nature, 541(7638), 516–520, doi:10.1038/nature20780, 2017.

909 Kampf, S., Markus, J., Heath, J. and Moore, C.: Snowmelt runoff and soil moisture dynamics on steep subalpine
910 hillslopes, Hydrol. Process., 29(5), 712–723, doi:10.1002/hyp.10179, 2015.

911 Keenan, T. F., Migliavacca, M., Papale, D., Baldocchi, D., Reichstein, M., Torn, M. and Wutzler, T.: Widespread
912 inhibition of daytime ecosystem respiration, Nat. Ecol. Evol., 3(3), 407–415, doi:10.1038/s41559-019-0809-2, 2019.

913 ~~Knowles, J. F., Burns, S. P., Blanken, P. D. and Monson, R. K.: Fluxes of energy, water, and carbon dioxide from~~
914 ~~mountain ecosystems at Niwot Ridge, Colorado, Plant Ecol. Divers., doi:10.1080/17550874.2014.904950, 2015.~~

915 ~~Knowles, J. F., Blanken, P. D. and Williams, M. W.: Wet meadow ecosystems contribute the majority of overwinter~~
916 ~~soil respiration from snow-scoured alpine tundra, J. Geophys. Res. G Biogeosciences, 121(4), 1118–1130,~~
917 ~~doi:10.1002/2015JG003081, 2016.~~

918 Kratzert, F., Klotz, D., Brenner, C., Schulz, K. and Herrnegger, M.: Rainfall–runoff modelling using Long Short-
919 Term Memory (LSTM) networks, Hydrol. Earth Syst. Sci., 22(11), 6005–6022, doi:10.5194/hess-22-6005-2018,
920 2018.

921 Lasslop, G., Reichstein, M., Papale, D., Richardson, A., Arneth, A., Barr, A., Stoy, P. and Wohlfahrt, G.: Separation
922 of net ecosystem exchange into assimilation and respiration using a light response curve approach: Critical issues
923 and global evaluation, Glob. Chang. Biol., 16(1), 187–208, doi:10.1111/j.1365-2486.2009.02041.x, 2010.

924 Livingston, G. P. and Hutchinson, G. L.: Enclosure-based measurement of trace gas exchange: applications and
925 sources of error., 1995.

926 Ma, Y., Liu, S., Song, L., Xu, Z., Liu, Y., Xu, T. and Zhu, Z.: Estimation of daily evapotranspiration and irrigation
927 water efficiency at a Landsat-like scale for an arid irrigation area using multi-source remote sensing data, Remote
928 Sens. Environ., 216(August), 715–734, doi:10.1016/j.rse.2018.07.019, 2018.

929 Main-Knorn, M., Pflug, B., Louis, J., Debaecker, V., Müller-Wilm, U. and Gascon, F.: Sen2Cor for Sentinel-2.,

930 [2017.](#)

931 McCabe, M. F., Aragon, B., Houborg, R. and Mascaro, J.: CubeSats in Hydrology: Ultrahigh-Resolution Insights
 932 Into Vegetation Dynamics and Terrestrial Evaporation, *Water Resour. Res.*, 53(12), 10017–10024,
 933 doi:10.1002/2017WR022240, 2017.

934 Metzger, S., Junkermann, W., Mauder, M., Butterbach-Bahl, K., Trancón Y Widemann, B., Neidl, F., Schäfer, K.,
 935 Wieneke, S., Zheng, X. H., Schmid, H. P. and Foken, T.: Spatially explicit regionalization of airborne flux
 936 measurements using environmental response functions, *Biogeosciences*, 10(4), 2193–2217, doi:10.5194/bg-10-
 937 2193-2013, 2013.

938 Migliavacca, M., Reichstein, M., Richardson, A. D., Mahecha, M. D., Cremonese, E., Delpierre, N., Galvagno, M.,
 939 Law, B. E., Wohlfahrt, G., Andrew Black, T., Carvalhais, N., Ceccherini, G., Chen, J., Gobron, N., Koffi, E.,
 940 William Munger, J., Perez-Priego, O., Robustelli, M., Tomelleri, E. and Cescatti, A.: Influence of physiological
 941 phenology on the seasonal pattern of ecosystem respiration in deciduous forests, *Glob. Chang. Biol.*, 21(1), 363–
 942 376, doi:10.1111/gcb.12671, 2015.

943 Mohanty, B. P., Cosh, M. H., Lakshmi, V. and Montzka, C.: Soil moisture remote sensing: State-of-the-science,
 944 *Vadose Zo. J.*, doi:10.2136/vzj2016.10.0105, 2017.

945 Mu, Q., Zhao, M. and Running, S. W.: MODIS Global Terrestrial Evapotranspiration (ET) Product
 946 (MOD16A2/A3), Algorithm Theor. Basis Doc., 2013.

947 NASA: Moderate Resolution Imaging Spectroradiometer (MODIS) Overview, Nasa, 2008.

948 Ng, G., Bedford, D. and Miller, D.: A mechanistic modeling and data assimilation framework for Mojave Desert
 949 ecohydrology, *Water Resour. Res.*, 4662–4685, doi:10.1002/2014WR015281.Received, 2014.

950 [Noormets, A., Desai, A. R., Cook, B. D., Euskirchen, E. S., Ricciuto, D. M., Davis, K. J., Bolstad, P. V., Schmid, H.](#)
 951 [P., Vogel, C. V., Carey, E. V., Su, H. B. and Chen, J.: Moisture sensitivity of ecosystem respiration: Comparison of](#)
 952 [14 forest ecosystems in the Upper Great Lakes Region, USA, *Agric. For. Meteorol.*, doi:10.1016/j.agrformet.2007.08.002, 2008.](#)

953 [doi:10.1016/j.agrformet.2007.08.002, 2008.](#)

954 Olah, C.: Understanding LSTM Networks, <https://colah.github.io/posts/2015-08-Understanding-LSTMs/>, 2015,
 955 2015.

956 Oleson, K. W., Lawrence, D. M., Bonan, G. B., Drewniak, B., Huang, M., Koven, C. D., Levis, S., Li, F., Riley, J.,
 957 Subin, Z. M., Swenson, S. C., Thornton, P. E., Bozbiyik, A., Fisher, R. A., Heald, C. L., Kluzek, E., Lamarque, J.-
 958 F., Lawrence, P. J., Leung, L. R., Lipscomb, W., Muszala, S., Ricciuto, D. M., Sacks, W. J., Sun, Y., Tang, J. and
 959 Yang, Z.-L.: Technical Description of version 4.5 of the Community Land Model (CLM), 2013.

960 Omernik, J. M.: Perspectives on the nature and definition of ecological regions., *Environ. Manage.*,
 961 doi:10.1007/s00267-003-5197-2, 2004.

962 Omernik, J. M. and Griffith, G. E.: Ecoregions of the Conterminous United States: Evolution of a Hierarchical
 963 Spatial Framework, *Environ. Manage.*, doi:10.1007/s00267-014-0364-1, 2014.

964 Oyler, J. W., Dobrowski, S. Z., Ballantyne, A. P., Klene, A. E. and Running, S. W.: Artificial amplification of
 965 warming trends across the mountains of the western United States, *Geophys. Res. Lett.*,
 966 doi:10.1002/2014GL062803, 2015.

967 Paca, V. H. da M., Espinoza-Dávalos, G. E., Hessels, T. M., Moreira, D. M., Comair, G. F. and Bastiaanssen, W. G.
 968 M.: The spatial variability of actual evapotranspiration across the Amazon River Basin based on remote sensing
 969 products validated with flux towers, *Ecol. Process.*, 8(1), doi:10.1186/s13717-019-0158-8, 2019.

970 [Pelletier, J. D., Barron Gafford, G. A., Gutiérrez Jurado, H., Hinekley, E. L. S., Istanbuluoglu, E., McGuire, L. A.,](#)
 971 [Niu, G. Y., Poulos, M. J., Rasmussen, C., Richardson, P., Swetnam, T. L. and Tucker, G. E.: Which way do you lean?](#)
 972 [Using slope aspect variations to understand Critical Zone processes and feedbacks, *Earth Surf. Process. Landforms*,](#)
 973 [doi:10.1002/esp.4306, 2018.](#)

974 [Pedersen, S. H., Liston, G. E., Tamstorf, M. P., Abermann, J., Lund, M. and Schmidt, N. M.: Quantifying snow](#)

975 [controls on vegetation greenness, *Ecosphere*, doi:10.1002/ecs2.2309, 2018.](#)

976 PRIESTLEY, C. H. B. and TAYLOR, R. J.: On the Assessment of Surface Heat Flux and Evaporation Using Large-
977 Scale Parameters, *Mon. Weather Rev.*, doi:10.1175/1520-0493(1972)100<0081:otaosh>2.3.co;2, 1972.

978 Pumpanen, J., Kolari, P., Ilvesniemi, H., Minkinen, K., Vesala, T., Niinistö, S., Lohila, A., Larmola, T., Morero,
979 M., Pihlatie, M., Janssens, I., Yuste, J. C., Grünzweig, J. M., Reth, S., Subke, J. A., Savage, K., Kutsch, W.,
980 Østreng, G., Ziegler, W., Anthoni, P., Lindroth, A. and Hari, P.: Comparison of different chamber techniques for
981 measuring soil CO₂ efflux, *Agric. For. Meteorol.*, doi:10.1016/j.agrformet.2003.12.001, 2004.

982 Qiao, Z., Xu, X., Zhao, M., Wang, F. and Liu, L.: The application of a binary division procedure to the classification
983 of forest subcategories using MODIS time-series data during 2000–2010 in China, *Int. J. Remote Sens.*,
984 doi:10.1080/01431161.2016.1176269, 2016.

985 Reichstein, M., Falge, E., Baldocchi, D., Papale, D., Aubinet, M., Berbigier, P., Bernhofer, C., Buchmann, N.,
986 Gilmanov, T., Granier, A., Grünwald, T., Havránková, K., Ilvesniemi, H., Janous, D., Knohl, A., Laurila, T., Lohila,
987 A., Loustau, D., Matteucci, G., Meyers, T., Miglietta, F., Ourcival, J. M., Pumpanen, J., Rambal, S., Rotenberg, E.,
988 Sanz, M., Tenhunen, J., Seufert, G., Vaccari, F., Vesala, T., Yakir, D. and Valentini, R.: On the separation of net
989 ecosystem exchange into assimilation and ecosystem respiration: Review and improved algorithm, *Glob. Chang.*
990 *Biol.*, doi:10.1111/j.1365-2486.2005.001002.x, 2005.

991 Reichstein, M., Camps-Valls, G., Stevens, B., Jung, M., Denzler, J., Carvalhais, N. and Prabhat: Deep learning and
992 process understanding for data-driven Earth system science, *Nature*, 566(7743), 195–204, doi:10.1038/s41586-019-
993 0912-1, 2019.

994 Ren, H., Cromwell, E., Kravitz, B. and Chen, X.: Using Deep Learning to Fill Spatio-Temporal Data Gaps in
995 Hydrological Monitoring Networks, *Hydrol. Earth Syst. Sci. Discuss.*, (May), 1–20, doi:10.5194/hess-2019-196,
996 2019.

997 Rungee, J., Bales, R. and Goulden, M.: Evapotranspiration response to multiyear dry periods in the semiarid western
998 United States, *Hydrol. Process.*, doi:10.1002/hyp.13322, 2019.

999 Ryu, Y., Baldocchi, D. D., Kobayashi, H., Van Ingen, C., Li, J., Black, T. A., Beringer, J., Van Gorsel, E., Knohl,
1000 A., Law, B. E. and Rouspard, O.: Integration of MODIS land and atmosphere products with a coupled-process
1001 model to estimate gross primary productivity and evapotranspiration from 1 km to global scales, *Global*
1002 *Biogeochem. Cycles*, 25(4), 1–24, doi:10.1029/2011GB004053, 2011.

1003 ~~Schimel, D., Kittel, T. G. F., Running, S., Monson, R., Turnipseed, A. and Anderson, D.: Carbon sequestration studied~~
1004 ~~in Western U.S. mountains, *Eos (Washington, DC)*, doi:10.1029/2002EO000314, 2002.~~

1005 Seneviratne, S. I., Lüthi, D., Litschi, M. and Schär, C.: Land-atmosphere coupling and climate change in Europe,
1006 *Nature*, doi:10.1038/nature05095, 2006.

1007 ~~Speckman, H. N., Frank, J. M., Bradford, J. B., Miles, B. L., Massman, W. J., Parton, W. J. and Ryan, M. G.: Forest~~
1008 ~~ecosystem respiration estimated from eddy covariance and chamber measurements under high turbulence and~~
1009 ~~substantial tree mortality from bark beetles, *Glob. Chang. Biol.*, doi:10.1111/geb.12731, 2015.~~

1010 ~~Sloat, L. L., Henderson, A. N., Lamanna, C. and Enquist, B. J.: The Effect of the Foresummer Drought on Carbon~~
1011 ~~Exchange in Subalpine Meadows, *Ecosystems*, 18(3), 533–545, doi:10.1007/s10021-015-9845-1, 2015.~~

1012 Strachan, S., Kelsey, E. P., Brown, R. F., Dascalu, S., Harris, F., Kent, G., Lyles, B., McCurdy, G., Slater, D. and
1013 Smith, K.: Filling the Data Gaps in Mountain Climate Observatories Through Advanced Technology, Refined
1014 Instrument Siting, and a Focus on Gradients, *Mt. Res. Dev.*, 36(4), 518–527, doi:10.1659/mrd-journal-d-16-00028.1,
1015 2016.

1016 Suleau, M., Moureaux, C., Dufranne, D., Buysse, P., Bodson, B., Destain, J. P., Heinesch, B., Debacq, A. and
1017 Aubinet, M.: Respiration of three Belgian crops: Partitioning of total ecosystem respiration in its heterotrophic,
1018 above- and below-ground autotrophic components, *Agric. For. Meteorol.*, doi:10.1016/j.agrformet.2011.01.012,
1019 2011.

Teuling, A. J., Van Loon, A. F., Seneviratne, S. I., Lehner, I., Aubinet, M., Heinesch, B., Bernhofer, C., Grünwald, T., Prasse, H. and Spank, U.: Evapotranspiration amplifies European summer drought, *Geophys. Res. Lett.*, doi:10.1002/grl.50495, 2013.

Thornton, P. E., Thornton, M. M., Mayer, B. W., Wei, Y., Devarakonda, R., Vose, R. S. and Cook, R. B.: Daymet: Daily Surface Weather Data on a 1-km Grid for North America, Version 3, ORNL DAAC, Oak Ridge, Tennessee, USA, 2017.

Tran, A. P., Rungee, J., Faybishenko, B., Dafflon, B. and Hubbard, S. S.: Assessment of spatiotemporal variability of evapotranspiration and its governing factors in a mountainous watershed, *Water (Switzerland)*, 11(2), doi:10.3390/w11020243, 2019.

U.S. Environmental Protection Agency: Level III Ecoregions of the Continental United States, *Environ. Prot.*, 2003.

Viviroli, D. and Weingartner, R.: “Water towers”—A global view of the hydrological importance of mountains, in *Advances in Global Change Research.*, 2008.

Viviroli, D., Dürri, H. H., Messerli, B., Meybeck, M. and Weingartner, R.: Mountains of the world, water towers for humanity: Typology, mapping, and global significance, *Water Resour. Res.*, 43(7), 1–13, doi:10.1029/2006WR005653, 2007.

Vogelmann, J. E., Howard, S. M., Yang, L., Larson, C. R., Wylie, B. K. and Van Driel, N.: Completion of the 1990s National Land Cover Data set for the conterminous United States from Landsat thematic mapper data and ancillary data sources, *Photogramm. Eng. Remote Sensing*, 2001.

Wainwright, H. M., Steefel, C., Trutner, S. D., Henderson, A. N., Nikolopoulos, E. I., Wilmer, C. F., Chadwick, K. D., Falco, N., Schaettle, K. B., Brown, J. B., Steltzer, H., Williams, K. H., Hubbard, S. and Enquist, B. J.: Satellite-derived foresummer drought sensitivity of plant productivity in Rocky Mountain headwater catchments: spatial heterogeneity and geological-geomorphological control, *Environ. Res. Lett.*, doi:10.1088/1748-9326/ab8fd0, 2020.

Wang, B., Zha, T. S., Jia, X., Wu, B., Zhang, Y. Q. and Qin, S. G.: Soil moisture modifies the response of soil respiration to temperature in a desert shrub ecosystem, *Biogeosciences*, 11(2), 259–268, doi:10.5194/bg-11-259-2014, 2014.

Webb, R. W., Fassnacht, S. R. and Gooseff, M. N.: Hydrologic flow path development varies by aspect during spring snowmelt in complex subalpine terrain, *Cryosphere*, 12(1), 287–300, doi:10.5194/tc-12-287-2018, 2018.

Wieder, W. R., Knowles, J. F., Blanken, P. D., Swenson, S. C. and Suding, K. N.: Ecosystem function in complex mountain terrain: Combining models and long-term observations to advance process-based understanding, *J. Geophys. Res. Biogeosciences*, doi:10.1002/2016JG003704, 2017.

Williams, C. A. and Albertson, J. D.: Soil moisture controls on canopy-scale water and carbon fluxes in an African savanna, *Water Resour. Res.*, doi:10.1029/2004WR003208, 2004.

Williams, M., Richardson, A. D., Reichstein, M., Stoy, P. C., Peylin, P., Verbeeck, H., Carvalhais, N., Jung, M., Hollinger, D. Y., Kattge, J., Leuning, R., Luo, Y., Tomelleri, E., Trudinger, C. and Wang, Y.-P.: Improving land surface models with FLUXNET data, *Biogeosciences Discuss.*, doi:10.5194/bgd-6-2785-2009, 2009.

Wilson, K. B., Hanson, P. J., Mulholland, P. J., Baldocchi, D. D. and Wullschleger, S. D.: A comparison of methods for determining forest evapotranspiration and its components: Sap-flow, soil water budget, eddy covariance and catchment water balance, *Agric. For. Meteorol.*, 106(2), 153–168, doi:10.1016/S0168-1923(00)00199-4, 2001.

Xiao, J., Ollinger, S. V., Frolking, S., Hurt, G. C., Hollinger, D. Y., Davis, K. J., Pan, Y., Zhang, X., Deng, F., Chen, J., Baldocchi, D. D., Law, B. E., Arain, M. A., Desai, A. R., Richardson, A. D., Sun, G., Amiro, B., Margolis, H., Gu, L., Scott, R. L., Blanken, P. D. and Suyker, A. E.: Data-driven diagnostics of terrestrial carbon dynamics over North America, *Agric. For. Meteorol.*, doi:10.1016/j.agrformet.2014.06.013, 2014.

Xu, L., Baldocchi, D. D. and Tang, J.: How soil moisture, rain pulses, and growth alter the response of ecosystem respiration to temperature, *Global Biogeochem. Cycles*, 18(4), 1–10, doi:10.1029/2004GB002281, 2004.

Xu, T., Guo, Z., Liu, S., He, X., Meng, Y., Xu, Z., Xia, Y., Xiao, J., Zhang, Y., Ma, Y. and Song, L.: Evaluating

1065 Different Machine Learning Methods for Upscaling Evapotranspiration from Flux Towers to the Regional Scale, J.
1066 Geophys. Res. Atmos., 123(16), 8674–8690, doi:10.1029/2018JD028447, 2018.

1067 Zhang, L., Potter, N., Hickel, K., Zhang, Y. and Shao, Q.: Water balance modeling over variable time scales based
1068 on the Budyko framework - Model development and testing, J. Hydrol., 360(1–4), 117–131,
1069 doi:10.1016/j.jhydrol.2008.07.021, 2008.

1070 Zhang, Y., Kong, D., Gan, R., Chiew, F. H. S., McVicar, T. R., Zhang, Q. and Yang, Y.: Coupled estimation of
1071 500 m and 8-day resolution global evapotranspiration and gross primary production in 2002–2017, Remote Sens.
1072 Environ., 222(May 2018), 165–182, doi:10.1016/j.rse.2018.12.031, 2019.

1073

1074 **Appendix**

1075

1076 **1. ET and R_{ECO} Estimation over Time at other Fluxnet sites**

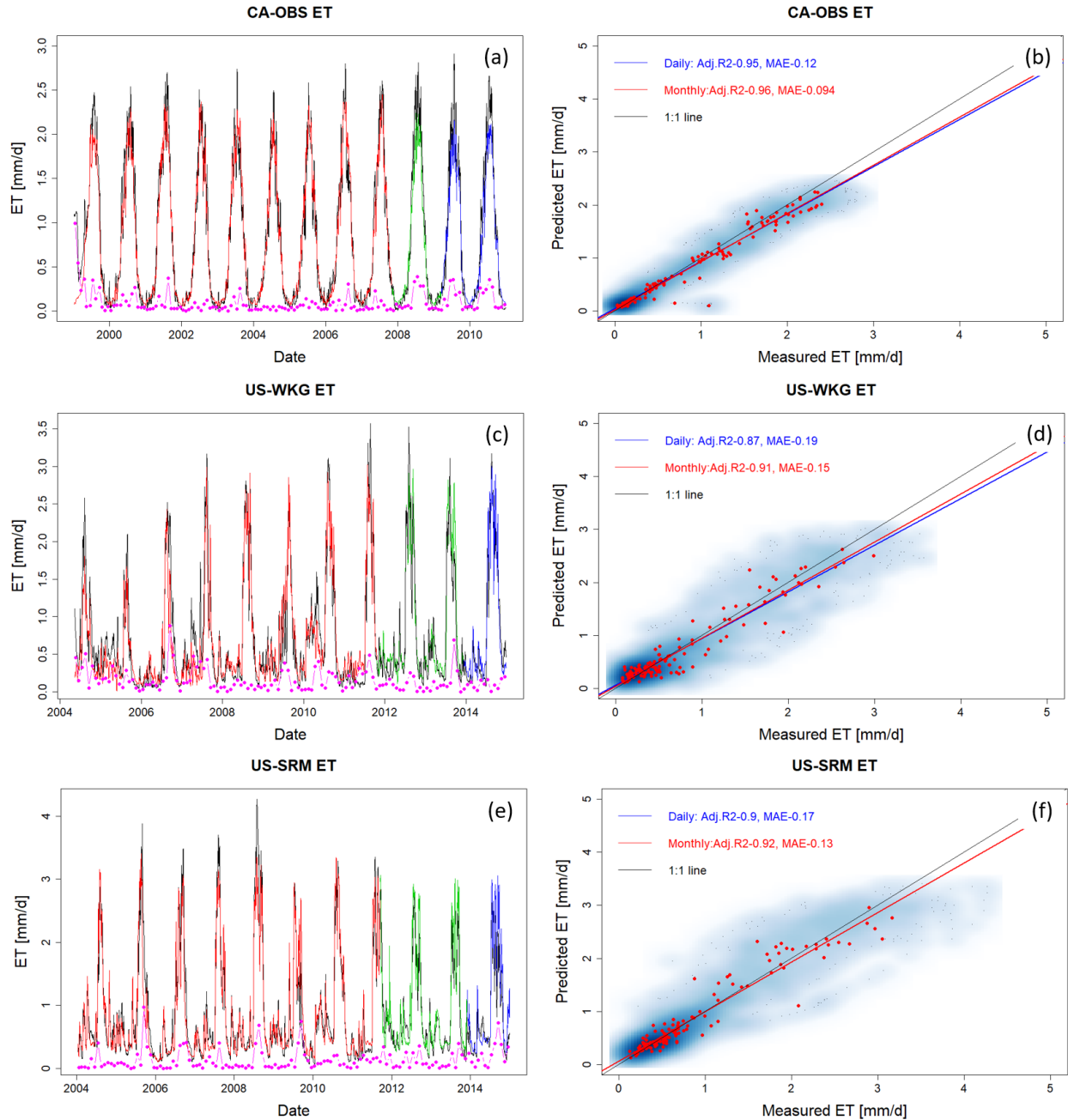


Figure A1: ET estimation with data from selected FLUXNET sites at CA-OBS, US-Wkg, and US-SRM. Panels (a), (c), and (e) present daily estimations of ET with red, green, and blue lines representing data used for training, validation, and prediction, respectively, and the black line representing the eddy covariance measurement. Pink points describe monthly mean difference between HPM estimation and measured data. Panels (b), (d), and (f) show the scatter plots of daily (blue) and monthly (red) ET. Darker blue clouds represent greater density of data points.

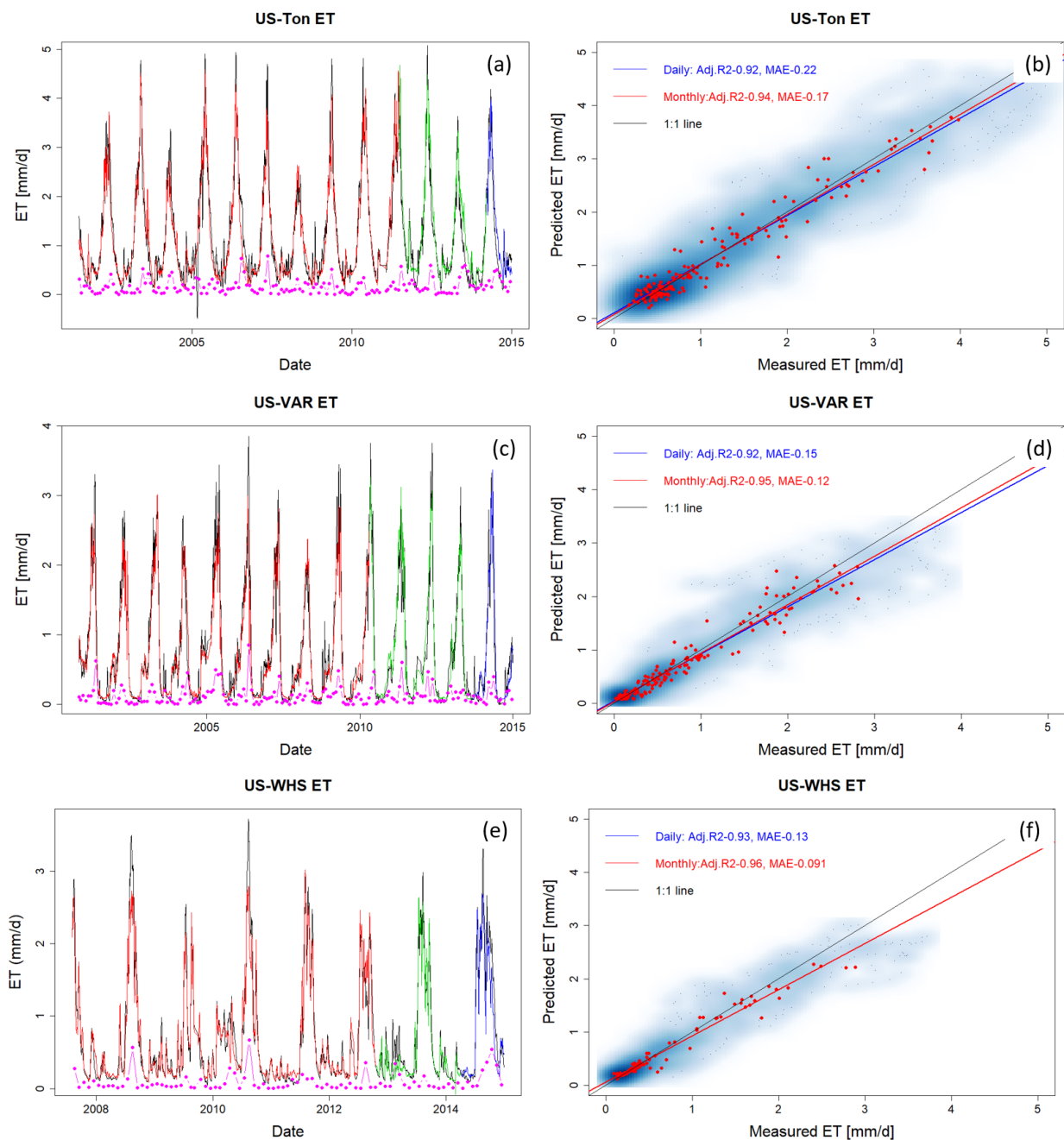


Figure A2: ET estimation with data from selected FLUXNET sites at US-Ton, US-Var, and US-Whs. Panels (a), (c), and (e) present daily estimations of ET with red, green, and blue lines representing data used for training, validation, and prediction, respectively, and the black line representing the eddy covariance measurement. Pink points describe monthly mean difference between HPM estimation and measured data. Panels (b), (d), and (f) show the scatter plots of daily (blue) and monthly (red) ET. Darker blue clouds represent greater density of data points.

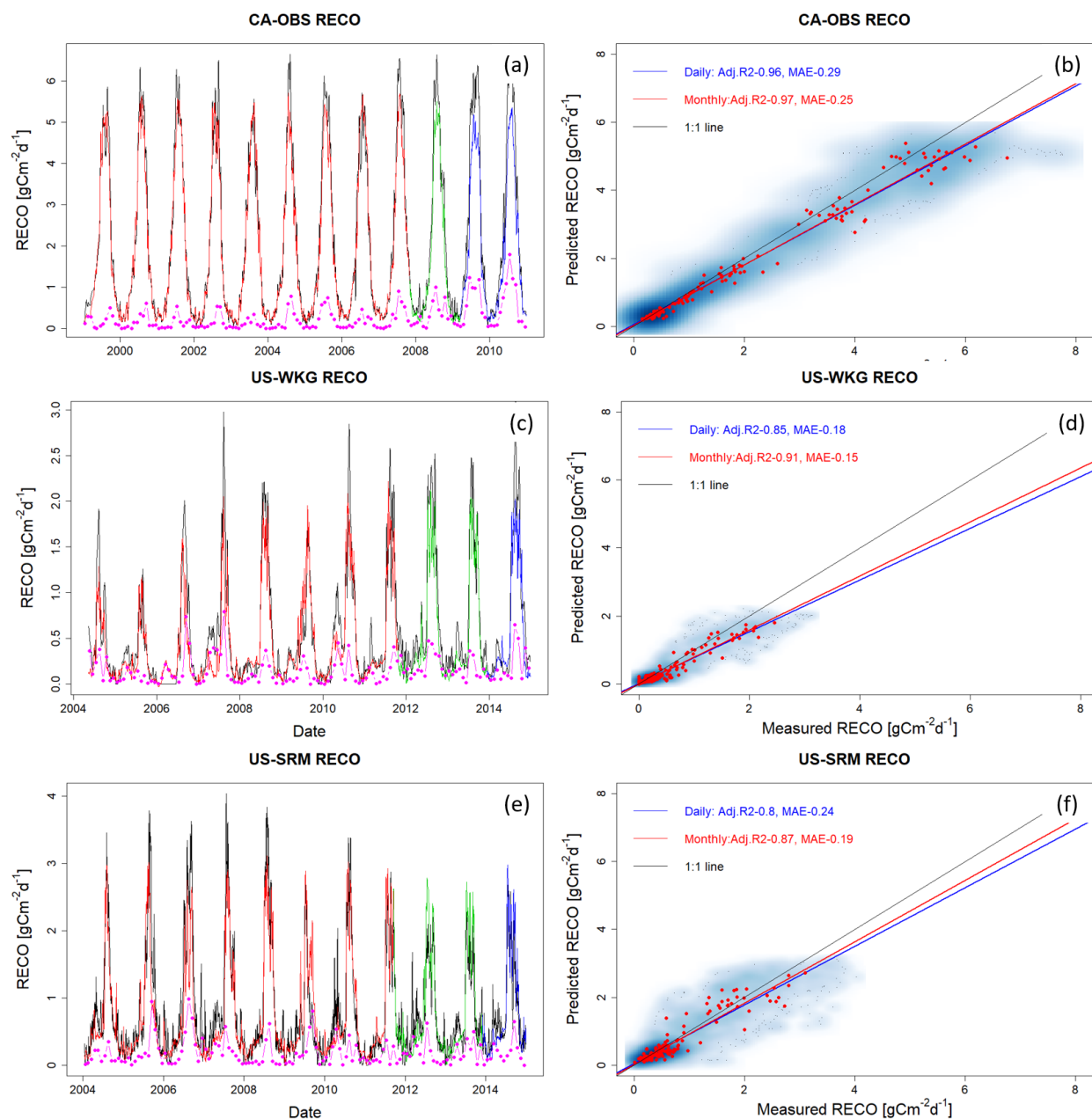


Figure A3: R_{ECO} estimation with data from selected FLUXNET sites at CA-OBS, US-Wkg, and US-SRM. Panels (a), (c), and (e) present daily estimations of R_{ECO} with red, green, and blue lines representing data used for training, validation, and prediction, respectively, and the black line is eddy covariance measurement. Pink points describe the monthly mean difference between HPM estimation and measured data. Panels (b), (d), and (f) show the scatter plots of daily (blue) and monthly (red) R_{ECO} . Darker blue clouds represent greater density of data points.

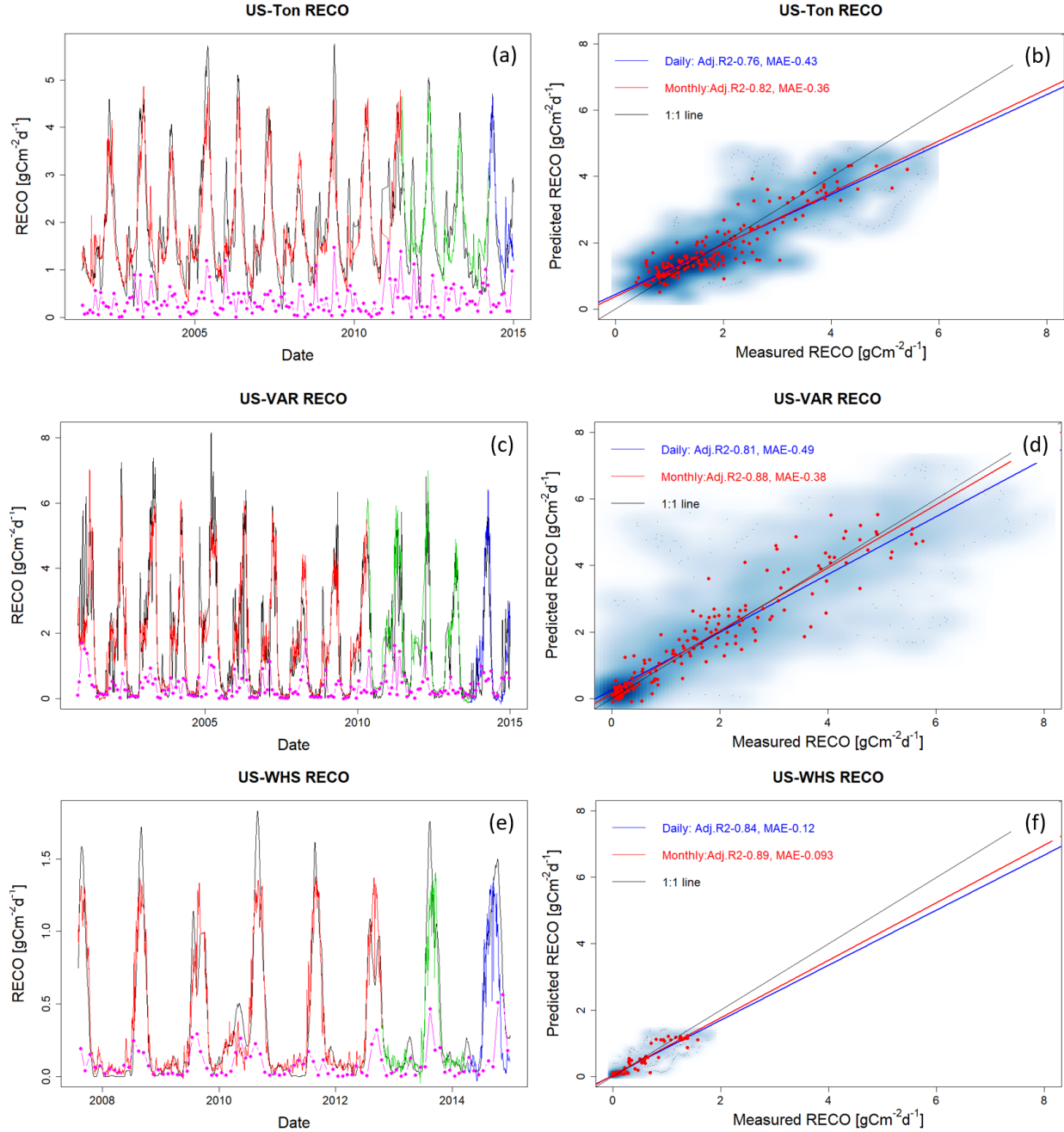


Figure A4: R_{ECO} estimation with data from selected FLUXNET sites at US-Ton, US-Var, and US-Whs. Panels (a), (c), and (e) present daily estimations of R_{ECO} with red, green, and blue lines representing data used for training, validation, and prediction, respectively, and the black line representing the eddy covariance measurement. Pink points describe monthly mean difference between HPM estimation and measured data. Panels (b), (d), and (f) show the scatter plots of daily (blue) and monthly (red) R_{ECO} . Darker blue clouds represent greater density of data points.

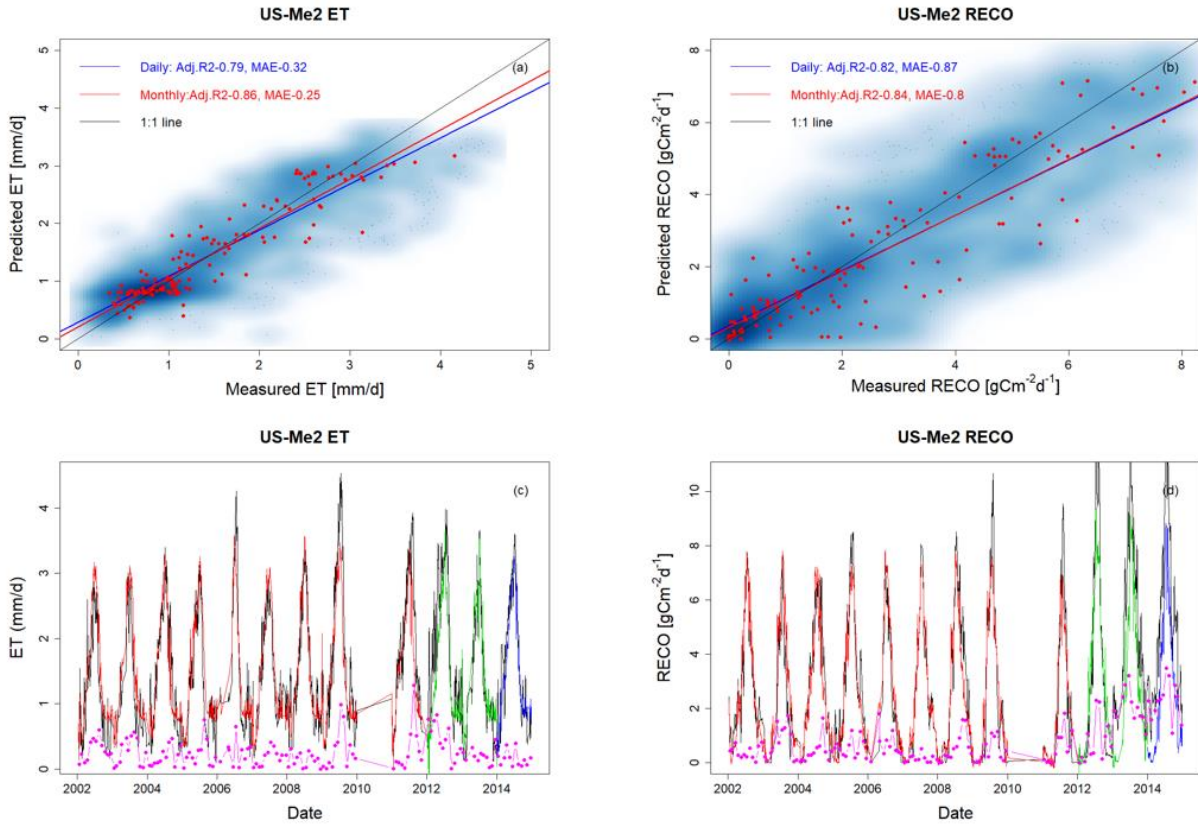


Figure A5: ET and R_{ECO} estimation at US-Me2. Panels (a) and (b) show the scatter plots of daily (blue) and monthly (red) ET and R_{ECO} . Darker blue clouds represent greater density of data points. Panels (c), and (d) present daily estimations of R_{ECO} with red, green, and blue lines representing data used for training, validation, and prediction, respectively, and the black line representing the eddy covariance measurement. Pink points describe monthly mean difference between HPM estimation and measured data.

2. Tested NEE Estimation over Time at CA-OAS and US-NR1

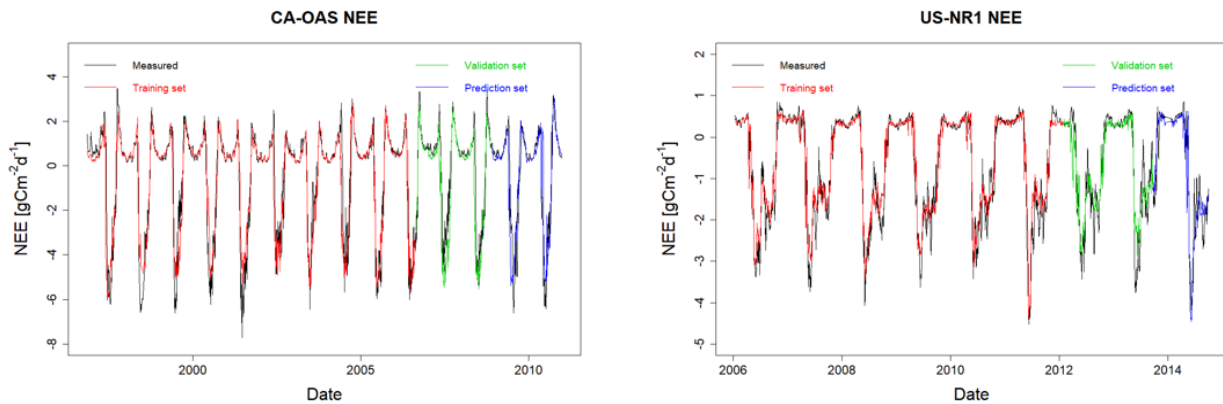


Figure A6. HPM estimate of NEE at CA-OAS and US-NR1. R^2 between estimation and measurements are 0.87, 0.83 and 0.81 at CA-OAS; 0.94, 0.88 and 0.90 at US-NR1 for the training set, validation set and prediction set, respectively. Model inputs include air temperature, soil temperature, sn, precipitation and radiation.